European Commission

JRC TECHNICAL REPORT

A non-destructive method to determine the neutron production rate of a sample of spent nuclear fuel under standard controlled area conditions

Schillebeeckx, P., Verwerft, M., Žerovnik, G., Parthoens, Y., Pedersen, B., Alaerts, G., Cools, G., Govers, K., Paepen, J., Varasano, G., Wynants, R.

2020

Joint Research Centre

EUR 30379 EN

EU Science Hub
https://ec.europa.eu/jrc

JRC121586

EUR 30379 EN

PDF ISBN 978-92-76-22349-8 ISSN 1831-9424 doi:10.2760/614853

Luxembourg: Publications Office of the European Union, 2020

How to cite this report: Schillebeeckx, P., Verwerft, M., Žerovnik, G., Parthoens, Y., Pedersen, B., Alaerts, G., Cools, G., Govers, K., Paepen, J., Varasano, G. and Wynants, R., *A non-destructive method to determine the neutron production rate of a sample of spent nuclear fuel under standard controlled area conditions,* EUR 30379 EN, Publications Office of the European Union, Luxembourg, 2020, ISBN 978-92-76-22349-8, doi:10.2760/614853, JRC121586.

Contents

Foreword

This work is part of the Work Package "Spent Fuel Characterisation and Evolution Until Disposal" of the European Joint Programme on Radioactive Waste Management (EURAD). It is part of deliverable 8.4 describing a system for non-destructive characterisation of nuclear spent fuel samples. The project leading to this deliverable has received funding from the European Union's Horizon 2020 research and innovation programme under grant agreement No 847593.

Acknowledgements

This work was partly funded by the European Union's Horizon 2020 Research and Innovation Programme under grant agreement No 847593. We are also indebted to the technical staff of the Laboratory for High and Medium level Activity of the SCK CEN for their assistance during the measurements and to Dr. P. Jansson (Uppsala University), Dr. M. Seidl (Preussen Elektra) and Dr. G. Van den Eynde (SCK CEN) for a careful review of the manuscript.

Authors

Peter Schillebeeckx, Marc Verwerft, Gašper Žerovnik, Yves Parthoens, Bent Pedersen, Gery Alaerts, Gerry Cools, Kevin Govers, Jan Paepen, Giovanni Varasano and Ruud Wynants

Abstract

A method to determine the neutron production rate of a sample of spent nuclear fuel by means of non-destructive analysis conducted under controlled-area conditions is described, validated and demonstrated. A standard neutron well-counter designed for routine nuclear safeguards applications is applied. The method relies on a transfer procedure that is adapted to the hot-cell facilities at the Laboratory for High and Medium level Activity of the SCK CEN. The sample transfer and measurement procedures are described together with results of Monte Carlo simulations. Experiments with radionuclide sources were carried out at the Joint Research Centre to test the procedures and to determine the performance characteristics of the detection device. Finally, measurements of a segment of a spent nuclear fuel rod were carried out at the SCK CEN to validate and demonstrate the method.

1 Introduction

Characterisation of spent nuclear fuel is essential in supporting a safe, secure, ecologic and economic handling, transport, interim storage and final disposal of spent nuclear fuel assemblies [1]-[4]. From operational safety perspectives, several quantities are of high importance: the source terms of interest for radiation protection are the neutron and γ-ray emission rates and spectra, the decay heat (due to all decay mechanisms) is required for spent nuclear fuel thermal performance and ageing assessment and the fissile inventory is one of the main drivers for criticality safety considerations and nuclear safeguards. Similar concerns drive the source term for the long-term safety assessment of disposal facilities. These source terms are determined by a complex inventory of nuclides with strongly varying characteristics [1]-[5]. Such an inventory and an evaluation of its evolution over the next thousands of years can only be obtained by theoretical calculations. Evidently, the theoretical calculations need to be validated and realistic confidence limits have to be determined [4], [6]. Both the validation and estimation of confidence limits require high quality experimental data. At present such data are primarily based on a combination of destructive chemical and radiochemical analysis methods [7]-[10], involving a series of steps including the dissolution of the sampled material [11]. Data obtained by Non-Destructive Analysis (NDA) are rather scarce. One of the objectives of the Work Package 8 Subtask 2 of the European Joint Programme on Radioactive Waste Management (EURAD) is to develop and improve state-of-the-art NDA methods to characterise Spent Nuclear Fuel (SNF) samples and assemblies [12]. These methods will be applied to provide accurate data for code validation and to provide recommendations for nuclear data that need to be improved [12].

In this report a procedure to measure non-destructively the neutron production rate of a SNF sample outside a hot cell under standard controlled area conditions is described, validated and demonstrated. The procedure relies on the hot cell infrastructures at the Laboratory for High and Medium level Activity (LHMA) of the Belgian nuclear research centre (SCK CEN). The procedure can be applied to any neutron counter that is optimised for neutron correlation measurements. The characteristics of the detection system together with the expected dose rates were estimated by Monte Carlo (MC) simulations. The results of the simulations were verified by experiments performed at the Joint Research Centre (JRC) and the SCK CEN) The results of this exercise serve as a first case demonstration that an SNF sample can be characterised by NDA methods outside a hot cell under standard controlled area conditions avoiding risks of contamination and excessive dose rates.

Theoretical estimations and examples of neutron production by SNF starting from UO_2 fresh fuel are discussed in section 2. The characteristics of the SNF segment sample that was measured are specified in section 3. Details about the detection system are given in section 4. The transfer container together with the procedures applied at the LHMA of SCK CEN are specified in section 5. Dose rates estimates based on measurements at JRC Ispra and the LHMA of SCK CEN are compared with results of calculations in section 6. The operating and performance characteristics of the detection system based on measurements with radionuclide sources are specified in section 7. The results of the measurements of the SNF segment sample are given in section 8. In section 9 the model that is used to analyse the data is explained and the final results are discussed. Section 10 provides a summary of the report and perspectives.

2 Theoretical considerations on neutron production by spent nuclear fuel

Neutron emission of SNF is due to spontaneous fission (sf) of actinides and (α, n) reactions in light nuclei. The total spatial-dependent neutron production rate $S_n(\vec{r}, \mathrm{t})$ as a function of cooling time (or time after end of irradiation) can be written as:

$$S_n(\vec{r}, \mathrm{t}) = \sum_j (s_{sf,j} + s_{\alpha,j})\, N_j(\vec{r}, t)\,, \tag{1}$$

with $N_j(\vec{r}, t)$ the spatially dependent number of nuclei (inventory) of nuclide j, $s_{sf,j}$ the specific neutron production rate per nucleus due to spontaneous fission of nuclide j and $s_{\alpha,j}$ the specific neutron production rate due to (α, n) reactions following the α-decay of nuclide j. The specific production rate due to spontaneous fission is given by:

$$s_{sf,j} = < \nu >_j \lambda_{sf,j}\,, \tag{2}$$

where $< \nu >_j$ is the average total number of neutrons produced per spontaneous fission of nuclide j and λ_{sfj} the decay constant for spontaneous fission of nuclide j. The specific neutron production rate due to α-decay of nuclide j is determined by:

$$s_{\alpha,j} = \lambda_{\alpha,j} \sum_l \sum_k P_j\left(E_{\alpha,k}\right) Y_l\left(E_{\alpha,k}\right)\,, \tag{3}$$

where $\lambda_{\alpha,j}$ is the decay constant for $\alpha-$decay of nuclide j, $P_j\left(E_{\alpha,k}\right)$ is the probability that an α-particle is produced with an energy $E_{\alpha,k}$ and $Y_l(E_{\alpha,k})$ is the total number of neutrons produced per incident α-particle with energy $E_{\alpha,k}$ interacting with nuclide l. The production of neutrons by (α, n) reactions is mostly treated under the assumption of an infinitely thick target, i.e. the thickness is sufficient to stop α-particles and prevent them from escaping the sample. Under these conditions the neutron yield Y_l can be calculated by:

$$Y_l(E_\alpha) = N_l \int_0^{E_\alpha} \frac{\sigma_l(E)}{\frac{dE}{dx}} dE\,, \tag{4}$$

where $\sigma_l(E)$ is the microscopic neutron production cross section for an α-particle with energy E interacting with a target nucleus l with a number volume density N_l and dE/dx is the linear stopping power of an α-particle in the target material.

Figure 1 shows the neutron production rate as a function of cooling time for a simulated UO_2 fuel sample with an initial ^{235}U enrichment of 4.8 wt%, which was irradiated in conditions typical for a Pressurised Water Reactor (PWR) to a Burnup (BU) of 50 GWd/t. The total production rate is plotted together with the contribution from spontaneous fission and (α, n) reactions. For cooling times below hundred years neutron emission in spent UO_2 fuel is dominated by spontaneous fission, mainly spontaneous fission of ^{244}Cm. For cooling times between 100 years and 500 years there is a relatively strong contribution from (α, n) reactions. This can also be concluded from Figure 2, which plots the relative contributions as a function of cooling time. The relative contributions to the total neutron production rate originating from spontaneous fission and (α, n) reactions due to the decay of specific nuclides, i.e. $^{238, 239, 240, 242}$Pu, ^{241}Am and $^{242, 244}$Cm, are plotted in Figure 3 and Figure 4, respectively. Neutron production due to spontaneous fission of ^{244}Cm represents the largest contribution for cooling times shorter than 80 years. The contribution from (α, n) reactions due to the decay of ^{238}Pu, ^{242}Cm and ^{241}Am is relatively small for such cooling times. For cooling times longer than 100 years, neutron emission is mainly due to spontaneous fission of $^{240, 242}$Pu and ^{246}Cm and (α, n) reactions following the decay of ^{241}Am and $^{238, 239, 240}$Pu.

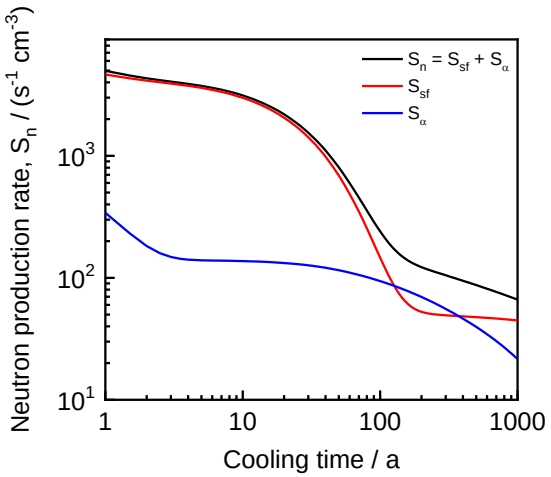

Figure 1. Total neutron production rate of a SNF sample as a function of cooling time together with the contribution due to spontaneous fission and (α, n) reactions in the fuel. The data are for a simulated UO_2 fuel sample with an initial ^{235}U enrichment of 4.8 wt% that was irradiated in conditions, typical for a PWR, to a burnup of 50 GWd/t. Data taken from Ref. [3].

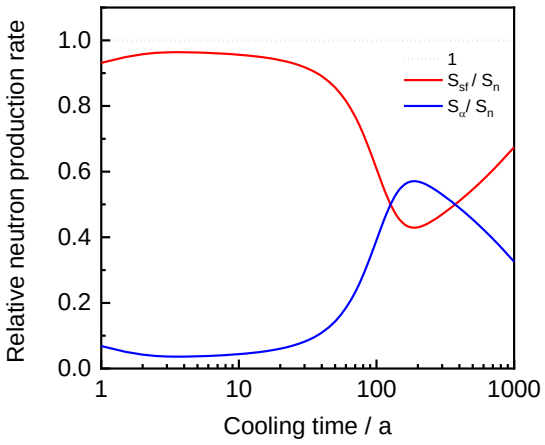

Figure 2. Relative contribution to the neutron production rate of prompt fission neutrons and neutrons created by (α, n) reactions in a SNF sample as a function of cooling time. The data are for a simulated UO_2 fuel sample with an initial ^{235}U enrichment of 4.8 wt% that was irradiated in conditions, typical for a PWR, to a burnup of 50 GWd/t. Data taken from Ref. [3].

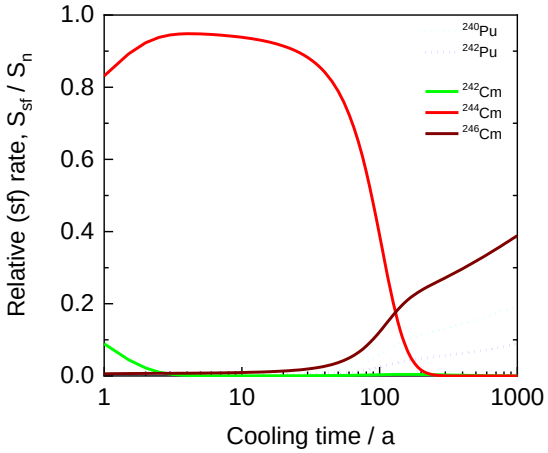

Figure 3. Relative contribution to the neutron production rate of prompt fission neutrons by $^{240,242}Pu$ and $^{242,244,246}Cm$ as a function of cooling time. The data are for a simulated UO_2 fuel sample with an initial ^{235}U enrichment of 4.8 wt% that was irradiated in conditions, typical for a PWR, to a burnup of 50 GWd/t. Data taken from Ref. [3].

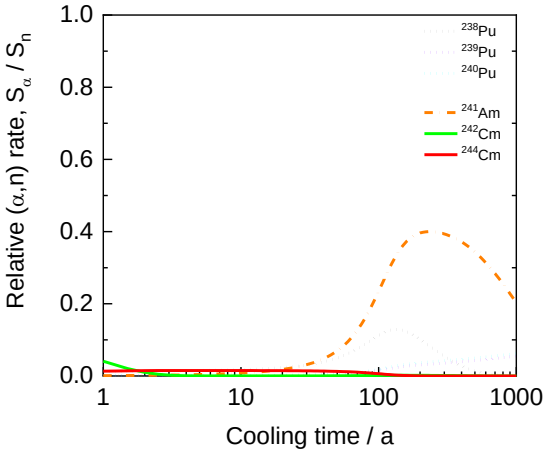

Figure 4. Relative contribution to the neutron production rate of (α, n) neutrons due to the α-decay of $^{238,239,240}Pu$, ^{241}Am and $^{242,244}Cm$ as a function of cooling time. The data are for a simulated UO_2 fuel sample with an initial ^{235}U enrichment of 4.8 wt% that was irradiated in conditions, typical for a PWR, to a burnup of 50 GWd/t. Data taken from Ref. [3].

For cooling times in the range of 2 – 50 years, neutron emission of spent UO_2 fuel is for more than 80 % dominated by spontaneous fission of ^{244}Cm and the neutron production rate can be used to estimate the ^{244}Cm inventory. Starting from fresh UO_2 fuel this curium isotope is produced through a sequence of successive neutron capture reactions and β^--decays. The different production paths are shown in Figure 5. The most probable path includes the production of ^{239}Pu by the $^{238}U(n, \gamma)$ reaction and involves six neutron induced capture reactions. The latter explains the strong dependence of the ^{244}Cm inventory of a SNF sample on the burnup, as illustrated in Figure 6. This figure plots the ^{244}Cm inventory starting from a UO_2 fresh fuel sample as a function of burnup for an initial enrichment of 4.8 wt%.

Due to the strong link between the neutron production rate and the ^{244}Cm inventory, the neutron production rate can be considered as a burnup indicator and as an experimental observable for nuclear safeguards applications to verify the plutonium content in spent fuel and reprocessed raffinates [13]. Absolute measurements of the neutron production rate of a SNF sample are rather scarce, if not, non-existing at all. In this work a procedure to measure the neutron production rate of a SNF sample relative to the one of a ^{252}Cf(sf) neutron source is proposed. The objective is to determine the neutron production rate and derive the ^{244}Cm inventory with a relative uncertainty of 2 %, which is close to or even better than the performance of radiochemical analysis methods [9], [10], [14]. The results of such neutron measurements are valuable data to validate the ^{244}Cm inventory derived by theoretical calculations.

Note that in this document uncertainties are quoted as standard uncertainties corresponding to a 68 % confidence interval.

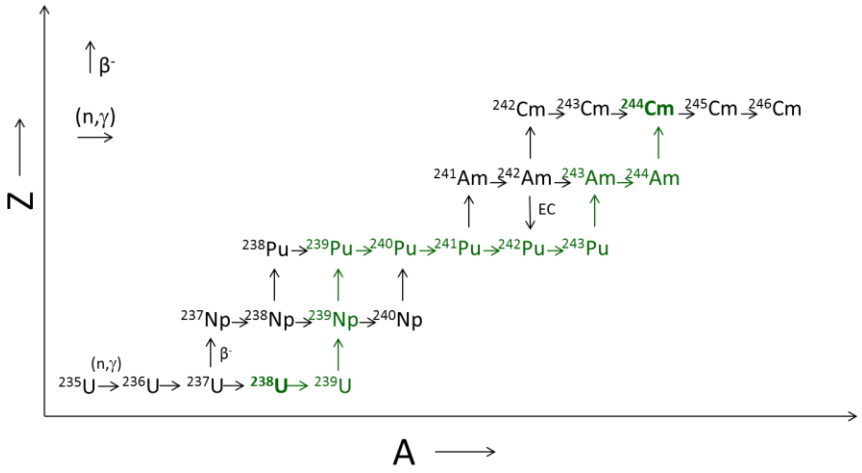

Figure 5. Schematic representation of the production path of ^{244}Cm by successive neutron capture reactions and β^--decays starting from the ^{238}U(n,γ) reaction. The main path is indicated in green.

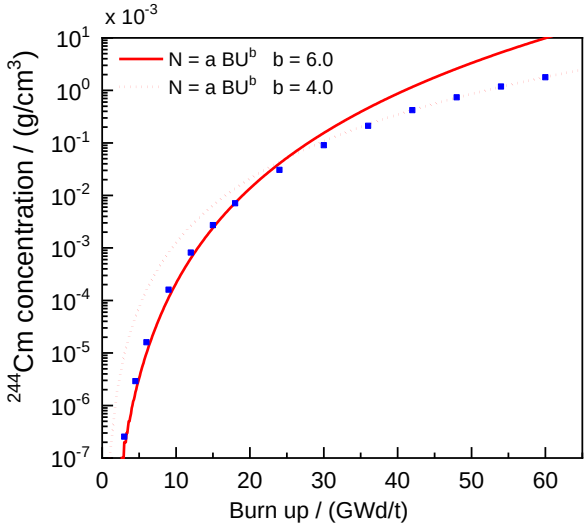

Figure 6. Inventory of ^{244}Cm as a function of burnup for a simulated UO_2 SNF sample with an initial ^{235}U enrichment of 4.8 wt% that was irradiated in conditions that are typical for a PWR. The inventory is approximated by two power functions with different exponents.

3 Characteristics of the analysed spent fuel segment

A segment was taken from a SNF rod irradiated in the Tihange 1 PWR during cycles 20 (April 1998 until August 1999) and 21 (September 1999 until 4 March 2001). The assembly FT1X57 from which the rod D05 was taken, was an AFA 2G assembly type manufactured by Areva. The geometry consists of a 15×15 array of fuel rods with 21 unfuelled locations (guide tubes) for insertion of control rods or instrumentation. It contains 188 UO_2 rods (4.5 wt% $^{235}U/U$) and 16 $(U,Gd)O_2$ fuel rods (10 wt% $Gd_2O_3/(U,Gd)O_2$ and 2 wt% $^{235}U/U$). Details of the irradiation history, fuel composition and geometry are reported in Ref. [15]. The rod average burnup, which was reconstructed from core mapping calculations and reactor power history, was calculated as slightly above 50 GWd/t. The axial variation of the burnup is evident from the results of a γ-ray scan performed as part of the post-irradiation examinations (see Figure 7 (a)). The burnup is almost independent of the position in the region between 750 mm and 3000 mm, apart from the regular depressions at grid positions (every 700 mm).

As a representative fuel rod for modern, high duty fuels, rod D05 has been used in various research and applied research projects, with samples taken for different types of investigations. The sampling in the axial region between 1750 mm and 2100 mm is represented in Figure 7 (b). Several leaching samples were used to investigate instant release of fission products under repository conditions [16], [17]. The results of microstructural analyses using a sample that was taken from the region between 1843 mm and 1854 mm are reported in Ref. [18]. A sample for a burnup analysis was taken from the region between 1819 mm and 1842 mm. The results of the BU analysis are reported in Ref. [19] and reproduced in Table 1. The uncertainty of the weighted average burnup is the combined standard uncertainty due to the sampling, weighing, dilution processes and nuclide inventory analysis. In the calculation of the weighted average of the burnup and its uncertainty the presence of common uncertainty components were taken into account.

The sample for the neutron measurements was taken from the region between 2056 mm and 2104 mm. The characteristics of this sample are reported in Table 2. The main uncertainty of the net mass of the fuel material is due to the uncertainty on the state of the cladding: uncertainty of the wall thickness, degree of oxidation and presence of deposits.

Table 1. Results of a radiochemical analysis of a SNF segment sample taken in the region between 1819 mm and 1842 mm. The nuclide inventory is expressed relative to the total weight of the fuel, i.e. including the oxygen. The burnup is expressed relative to the total amount of heavy metal, i.e. the fraction of heavy metal in the fuel. The cumulative fission yields used to calculate the BU are specified in the third column. The BU values are derived from the inventory assuming 200 MeV/fission The uncertainties of the BU are only due to those of the nuclide inventory. Details about this analysis are given in Ref. [20].

BU indicator	Date of analysis	Nuclide inventory mg/g	Cumulative fission yield (x 100)	Burnup GWd/t
^{137}Cs	10/21/2013	1.288 (28)	6.334	52.6 (11)
^{143}Nd + ^{144}Nd	02/05/2014	3.029 (32)	10.158	53.95 (56)
^{145}Nd + ^{146}Nd	02/05/2014	1.962 (21)	6.479	53.05 (56)
^{148}Nd	02/05/2014	0.534 (12)	1.724	53.3 (12)
^{150}Nd	02/05/2014	0.257 (11)	0.836	52.2 (23)
				Average: 52.78 (37)

Table 2. Characteristics of the SNF segment sample that was used for the neutron measurements at the LHMA facilities of SCK CEN.

Parameter	
Length	52.01 (4) mm
Segment weight	42.616 (1) g
Cladding weight	6.71 (4) g
Net fuel weight	35.91 (4) g

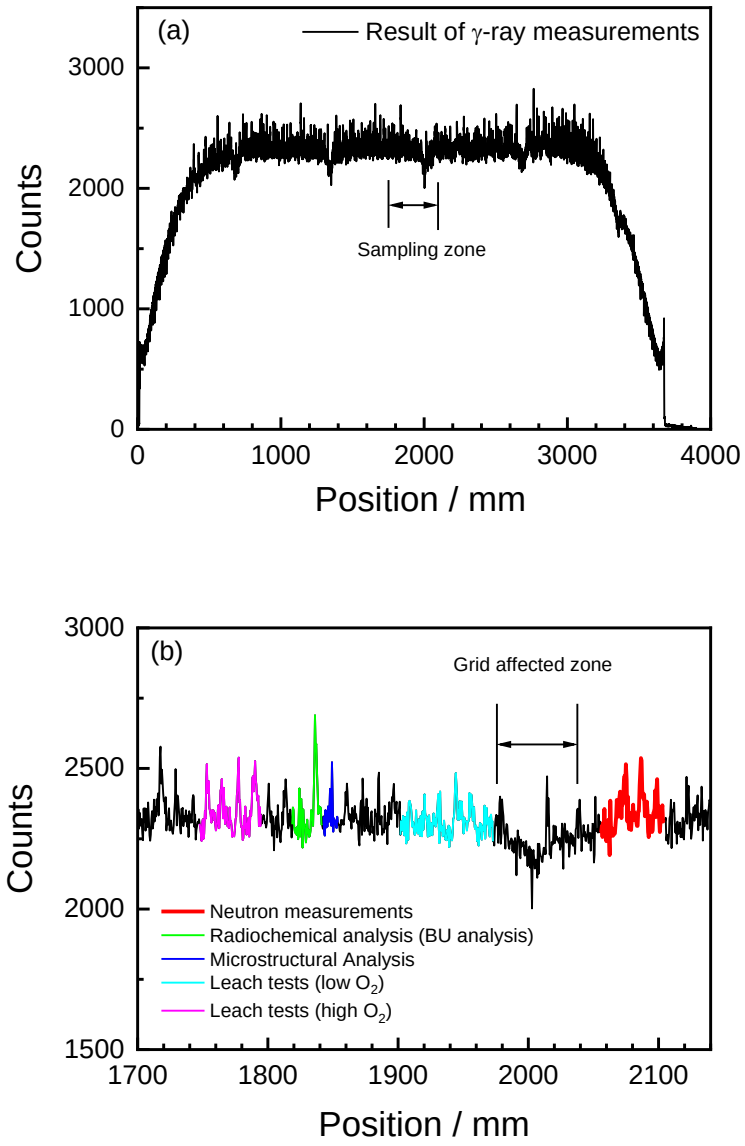

Figure 7. (a) Result of a total γ-ray scanning measurement of rod D05. The measurements were performed 2 years after the end of irradiation / end of life. The regular peaking pattern observed in the high BU part of the rod, between 750 mm and 3250 mm, is due to local migration of Cs to the pellet-pellet interfaces. Grid positions are clearly distinguished every 700 mm. (b) Results of a γ-ray scanning measurement in the axial region between 1700 mm and 2150 mm. The samples taken for different types of investigations are indicated with colours. The pellet-pellet interfaces and grid affected zone are clearly distinguished. The axial positions are relative to the bottom end of the fuel rod.

4 Neutron detection system

The neutron detection system was a transportable neutron well-counter that is routinely used for nuclear safeguards verification measurements. The detector was constructed in the 90s at JRC-Ispra for the assay of bulk samples containing uranium. The design was based on an Active Well Coincidence Counter (AWCC) device developed at the Las Alamos National Laboratory (LANL) [21]. Unfortunately, technical drawings, design specifications and data sheets of e.g. the neutron detectors are not available.

The counter has an overall length of 71.5 cm and an external diameter of 47.7 cm. The sample cavity has a diameter of 22.5 cm and height of 25.4 cm. The top and bottom plugs are made from polyethylene. The sample cavity is covered with a 0.4 mm thick sleeve of cadmium. Another cadmium sleeve is placed on the outside of the detector to reduce background contributions from ambient neutrons. A schematic representation of the counter is shown in Figure 8.

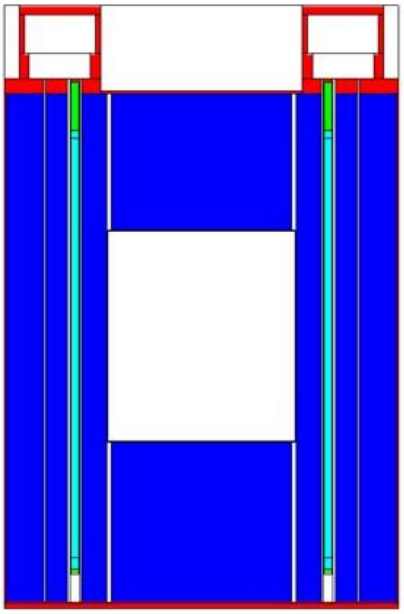

Figure 8. Schematic representation of the neutron counter which was designed and constructed at JRC-Ispra based on an AWCC device developed at LANL [21].

The detector consists of two concentric rings of 42 ^{3}He proportional counters embedded in polyethylene that is used as a neutron moderator. The counters are arranged in two concentric rings containing each 21 ^{3}He gas proportional counters. They are divided into six groups of seven counters. Each group is connected to one Amptek A111 hybrid charge sensitive preamplifier, discriminator and pulse shaper board [22]. Three boards are connected to three counters of the inner ring and four of the outer ring and three boards are connected to four counters of the inner ring and three of the outer ring, as illustrated in Figure 9.

The logic output of each board is sent to a counter/timer device and to an OR gate. The output of the OR gate can be used as an input for any shift register type of instrumentation or data acquisition system that registers the time of arrival of each detected event. For the measurements reported in this work a CAEN DT5751 digitiser [24] and a JSR-12 shift register [25] were used. The former produced list mode data of the time of arrival of each detected event and was used to register Rossi-alpha spectra. The JSR-12 shift register is based on a concept developed by Böhnel [26]. It records the total number of detected events together with the number of events that are detected in two time windows with an equal width, which are opened by each detected event. The width of these windows, referred to as the gate width, is denoted by t_g. The first gate is opened at a short time after each detected event. This time or predelay is represented by t_p. Its content, mostly referred to as 'Reals + Accidentals' or 'R+A', is due to a contribution of real coincident events (e.g. in case of a fission source) and accidental coincident events. The second gate is opened at a very long time delay after the first gate. Its content provides a direct measure of the accidental coincident events. The totals and reals rate, denoted by T and R, respectively, are also known as singlets and doublets (see e.g. Refs. [27]-[30]).

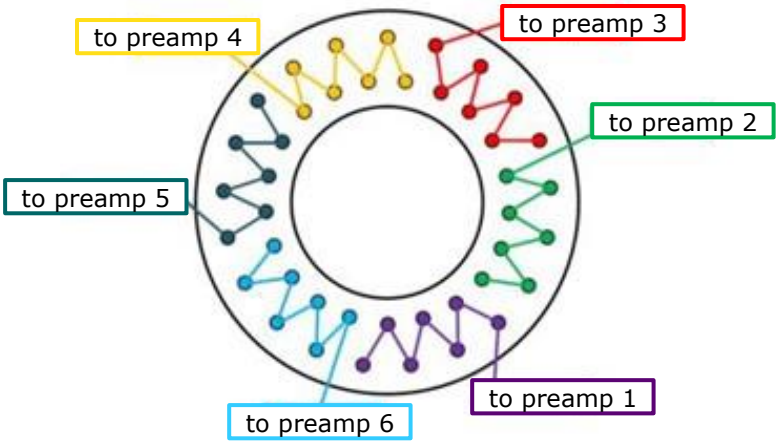

Figure 9. Schematic representation of the grouping of the detectors and their connection to an Amptek A111 hybrid charge sensitive preamplifier, discriminator and pulse shaper board (figure taken from Ref. [23]).

5 Sample transfer containers and procedure

Hot cell facilities are often not suited to accommodate a detection system as described in the previous section. Therefore, a dedicated procedure was developed to transfer a SNF sample from a hot cell to the neutron detection system eliminating the risk of contamination and minimising the radiation exposure of staff. A series of mandatory requirements had to be respected:

- the SNF sample should be large enough such that the data does not suffer from limited counting statistics;
- γ-ray shielding should be sufficient to allow a clear separation between the events resulting from the detection of a neutron and a γ-ray (γ-pile up);
- γ-ray shielding should be sufficient such that loading and unloading operations can be performed without exposure risk of staff performing these operations;
- the SNF sample should be encapsulated such that release of radionuclides to the environment is impossible;
- the encapsulated sample should be free of surface contamination;
- the entire process (sampling, encapsulation, loading in the neutron detector, measurement, and unloading) should be fully compliant with applicable safety regulations.

Additional optional requirements are to minimise additional countermeasures during data acquisition and to allow repeated background, calibration and sample measurements.

It was decided to work out a simple, yet effective multi-barrier encapsulation, consisting of four layers: two layers to minimise risks of spreading contamination and two other barriers to reduce the impact of the γ-ray radiation. The fuel rod segment was first loaded in a stainless steel capsule with tight sealing, enabling ultrasonic cleaning of the outer surface. After cleaning and verification of residual surface contamination, the capsule was loaded in a second aluminium can with a magnetic screw cap enabling easy manipulation to load the sample in and remove it from a GT-75 transport container of the SCK CEN. To increase the γ-ray shielding, the GT-75 container was pre-loaded with a sleeve made of a high-density tungsten base alloy (DENAL®). A schematic illustration of the multi-barrier encapsulation is shown in Figure 10.

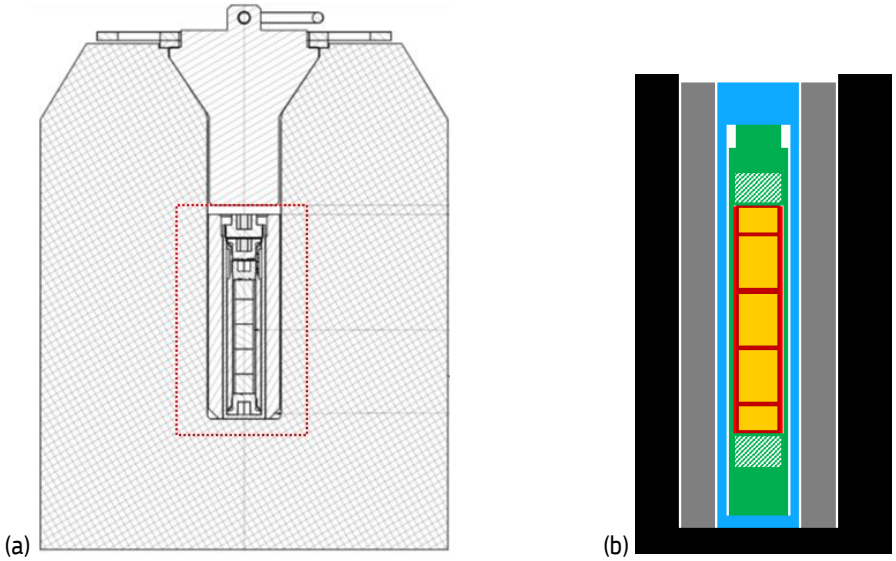

Figure 10. Part (a) is a technical drawing of the GT-75 transport container of SCK CEN loaded with the SNF sample placed in the stainless steel and aluminium container. Part (b) represents the different encapsulation and shielding layers. The colour coding is as follows: orange/red for the SNF sample; green for the stainless steel capsule; blue for the aluminium capsule; grey for the DENAL® sleeve and black for the lead shielding.

The GT-75 container, equipped with lifting eye bolts, was adapted to fit in the cavity of the neutron detector, as shown in Figure 11. Dimensioning of all components was performed such that optimal measurement conditions were met in terms of dose rates, compatibility with the neutron counter cavity, safety of the handling operations and compliance with operation restrictions. Prior to any operation, the expected dose rate for all handling operations and the dose rates during the measurements, were calculated on the basis of a SNF nuclide inventory and design data of the detection device and transfer containers. The results of these calculations together with results of dose rate measurements are discussed in the next section.

The handling sequence consisted of:

- precise cutting of a SNF segment sample to the required length;
- accurate weighing of the SNF segment sample;
- loading of the SNF segment sample in the stainless-steel capsule, cleaning and contamination control;
- loading in the aluminium capsule and contamination control;
- loading in the lead shielded container, foreseen with DENAL® sleeve and radiation level control during manipulation;
- loading of the container in the neutron detector cavity and control of static radiation level during data acquisition.

Unfortunately, only one GT-75 container was available such that it was not possible to perform a sequence of repeated background, calibration and SNF segment sample measurements.

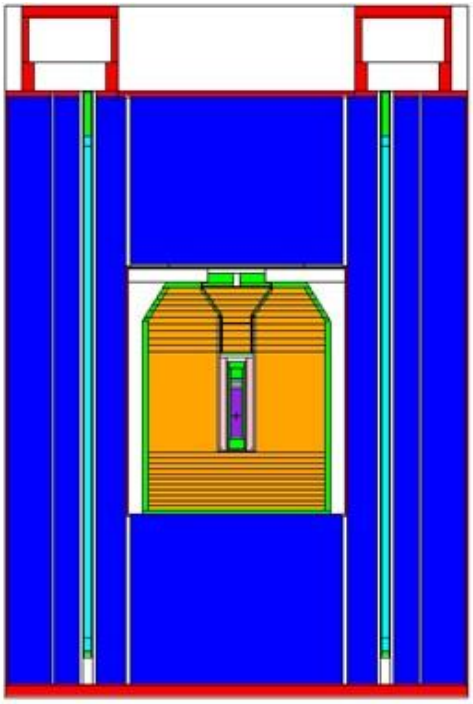

Figure 11. Schematic representation of the final configuration for the measurements of a SNF segment sample under standard controlled area conditions with the SNF segment sample in the transfer and GT-75 transport container.

6 Dose rates

The effectiveness of the multi-barrier encapsulation described in the previous section was verified by measurements with a ^{137}Cs radionuclide source at the PERLA laboratory of JRC-Ispra. The source, with a claimed nominal activity of 8 GBq, was put in a tungsten container before it was the transferred into the GT-75 container. The latter was placed inside the AWCC device as shown in Figure 12. The position of the ^{137}Cs source is indicated with a green dot. Due to the external dimensions of the tungsten container there was not enough space to place the Pb tap that closes the GT-75 container. Dose rate measurements were carried out at the outer surface of the device, as indicated by the red dots in Figure 12, and at 1 m distance from the side. The results of these measurements are compared in Table 3 with dose rates derived from Monte Carlo (MC) simulations with MCNP [31]. The dose rates were estimated using the photon fluence to absorbed dose conversion factors recommended by the International Commission on Radiological Protection (ICRP) [32], and assuming a weighting factor 1 between the equivalent dose and absorbed dose. The calculated dose rates are about a factor 2 lower compared to the measured ones. This systematic difference is most likely due to the declared activity of the source. Unfortunately, no activity certificate was available for the ^{137}Cs source. Evidently, differences due to limitations of the calculations cannot be excluded.

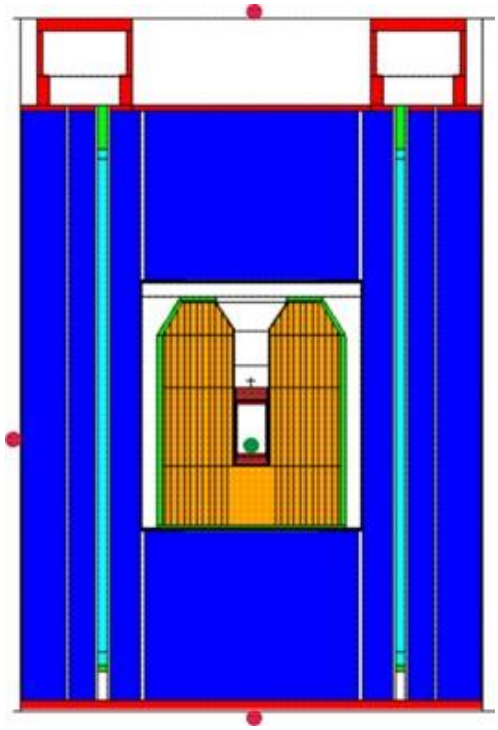

Figure 12. Schematic representation of the conditions for the dose rate estimations with a ^{137}Cs source. The source is placed in a tungsten container and the GT-75 container. The position of the source is indicated with a green dot and the measurement positions with red dots. Note that there was no place to close the GT-75 container with the Pb tap.

Table 3. Comparison of the measured (E) and calculated (C) dose rates at the outer surface of the neutron detector device and at 1 m distance from the side. The data are for a ^{137}Cs radionuclide source with a declared activity of 8 GBq placed in a tungsten container and the GT-75 container. Uncertainties due to number of simulated events can be neglected.

Position	Measured dose rate (E)	Calculated dose rate (C)	C/E
top	180 µSv/h	90 µSv/h	0.50
side	1.5 µSv/h	0.80 µSv/h	0.53
bottom	1.5 µSv/h	0.75 µSv/h	0.50
side at 1 m	0.5 µSv/h	0.35 µSv/h	0.70

The results of the measurements and calculations were used to define an ALARA procedure for measurements with a SNF segment sample at the LHMA laboratories of SCK CEN. In the ALARA procedure, conservative dose rates were considered by multiplying the calculated dose rates by a factor 2. The procedure covered the transport of the SNF sample from the hot cell to the neutron counter using the GT-75 container and subsequent measurements following the procedures described in the previous section. Dose rates were calculated for a UO_2 SNF sample of 36 g that was irradiated in conditions, typical for a PWR, to a burnup of 50 GWd/t with a cooling time of 17.5 years. These conditions are based on the fuel irradiation history of the SNF sample described in section 3. The calculated dose rates were derived from a combination of stochastic calculations with SERPENT [33], [34] and MCNP [31]. SERPENT was used to calculate the nuclide inventory of the SNF sample and MCNP to perform the γ-ray transport. Dose rates were calculated at the outer surfaces of the container and detection device and at a 1 m and 5 m distance from the container and detection device. The results are summarised in Table 4. Permission to perform the operations and measurements with the SNF segment sample was granted on the basis of these data.

Table 4. Calculated dose rates at the outer surface of the GT-75 container and neutron detector device (top, side and bottom) and at 1 m and 5 m distance from the side for a SNF sample with similar characteristics as the one described in section 3. Uncertainties due to number of simulated events can be neglected.

Position	GT-75 container	Neutron detection device
	Calculated dose rate	Calculated dose rate
Top	90 µSv/h	1.2 µSv/h
Side	270 µSv/h	7.0 µSv/h
Bottom	500 µSv/h	9.0 µSv/h
at 1 m (side)	0.45 µSv/h	0.20 µSv/h
at 5 m (side)	0.02 µSv/h	0.01 µSv/h

A measurement campaign with the SNF segment sample described in section 3 was organised at the LHMA laboratory of the SCK CEN. The experiments to determine the neutron emission rate lasted about three days. The results of these measurements are reported in section 8. The dose rates at the outer surface of the GT-75 container containing the sample were verified before the container was placed in the neutron detection device. The measurement points are shown in Figure 13. The results, which are reported in Table 5, are in good agreement with the calculated data. The dose rates are mainly due to γ-rays following the decay of ^{137}Cs and ^{154}Eu. The data in Table 5 show that at 1 m distance from the device the dose rates are well below 2 µSv/h such that no extreme dose-mitigating measures were required.

When the experiments to determine the neutron emission rate of the SNF sample were finalised the SNF segment sample was transported back to the hot cell. The GT-75 container was removed from the hot cell and swipe tests were performed at the inside and outside of the GT-75 transport container. The results of these tests did not show any evidence of a residual contamination of the GT-75 container. Hence, this measurement campaign demonstrated that NDA experiments with a SNF sample can be carried out under standard controlled area conditions without exposure risks of staff performing the operations or measurements, avoiding release of radionuclides to the environment and keeping the outside of the aluminium container free from surface contamination.

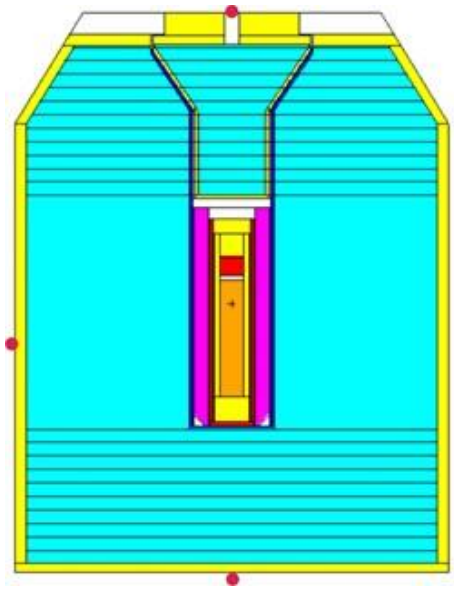

Figure 13. Schematic representation of the dose rate measurements with the SNF segment sample placed in the transfer and GT-75 transport containers. The measurement positions are indicated by a red dot.

Table 5. Measured and calculated dose rates at the outer surface of the GT-75 container. The conservative dose rates adopted in the ALARA procedure for the SNF sample measurements at the LHMA laboratories of SCK CEN are also given. The dose rates are for a SNF sample with similar characteristics as the one described in section 3.

Position	Measured dose rate	Calculated dose rate	Conservative dose rate
top	120 µSv/h	90 µSv/h	180 µSv/h
side	300 µSv/h	270 µSv/h	540 µSv/h
bottom	1000 µSv/h	500 µSv/h	1000 µSv/h

7 Operating and performance characteristics of the detection system

Experiments with radionuclide sources were carried out at JRC-Geel and JRC-Ispra to determine the operating and performance characteristics of the neutron detection device including the transfer and transport containers described in section 5. Measurements were performed using AmBe(α, n) sources with certified intensities, ^{252}Cf(sf) sources and a ^{137}Cs source with a nominal activity of 8 GBq. Operating characteristics

7.1 High voltage

The performance of each ^{3}He proportional counter was verified by recording the pulse height spectrum taken with a ^{241}AmBe(α, n) source. Experiments were carried out connecting each counter to a conventional electronics chain consisting of a pre-amplifier, spectroscopic amplifier and analog-to-digital convertor to verify both the performance of each proportional counter and the settings of the Amptek A111 board. The conventional electronics chain was connected to a data acquisition system developed at JRC-Geel [35].

The operating voltage was set at 2100 V. The source was placed in the centre of the detector cavity in the conditions of Figure 8, i.e. without transfer and GT-75 transport containers. The pulse height spectra taken in these conditions are very similar, as shown in Figure 14. This suggests that all counters have similar characteristics, i.e. anode wire diameter and ^{3}He gas pressure. The spectra obtained by summing the results for counters that are connected to the same Amptek A111 board are compared in Figure 15. This figure illustrates that for a fixed amplification the detectors can be operated with the same high voltage and discriminator conditions.

The optimum operating voltage with the counters connected to the Amptek A111 board was verified by recording the counts as a function of high voltage using the same AmBe source. The results are compared in Figure 16. The figure reveals for each group a clear plateau between 2000 V and 2200 V and suggests an optimum high voltage of about 2100 V for each group of counters. The results obtained with the A111 board are fully consistent with those obtained with the conventional electronics chain, which are obtained in almost ideal operating conditions. This is illustrated in Table 6 which compares the total counts obtained with the two systems for the same measurement conditions with the counters operated at 2100 V. The counts for the measurements with the conventional electronics are derived by integrating the amplitude spectrum applying a lower amplitude limit as indicated in Figure 15.

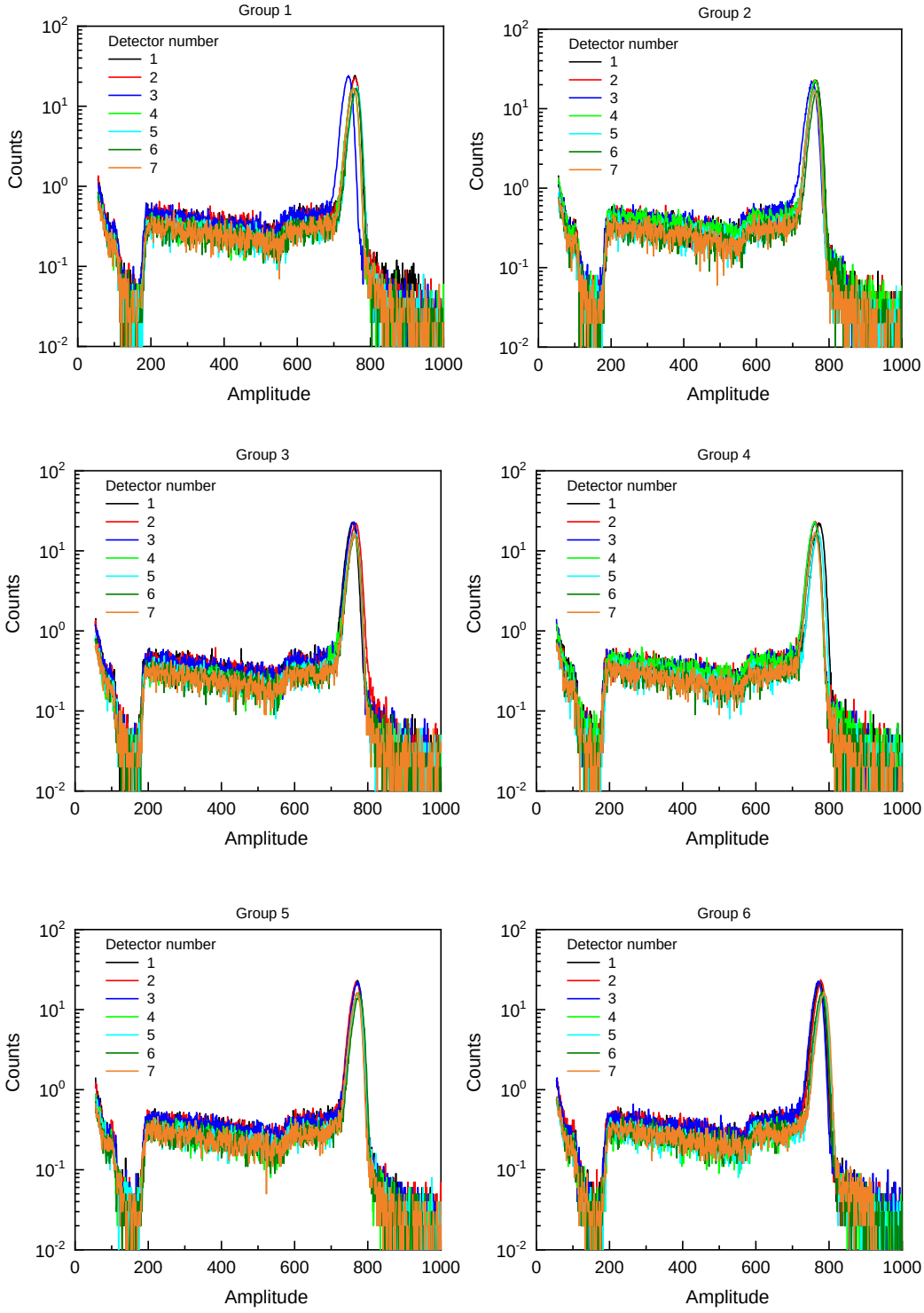

Figure 14. Amplitude spectra for each of the 42 ^{3}He proportional counters. The spectra are taken with an AmBe(α, n) neutron source in the centre of the cavity of the device in the configuration of Figure 8. Each figure shows the spectra for a set of counters that are connected to the same A111 board. All spectra were taken with the same total measurement time.

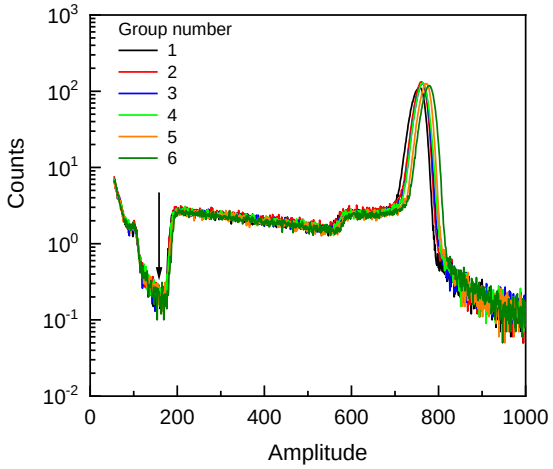

Figure 15. Amplitude spectra for the six groups of 7 proportional counters. The spectra are taken with an AmBe(α, n) neutron source in the centre of the cavity of the device in the configuration of Figure 8. The arrow indicates the lower integration limit used to calculate the total detected counts. All spectra were taken with the same total measurement time.

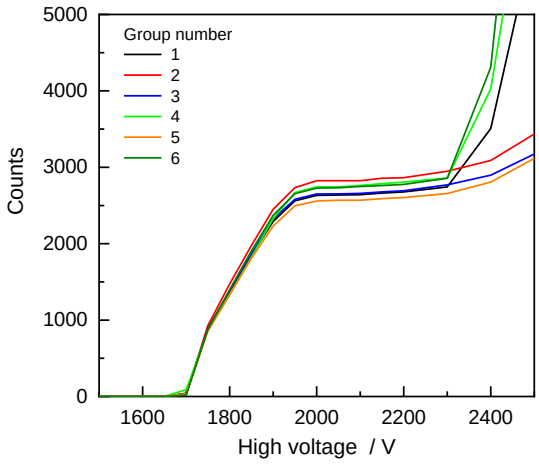

Figure 16. Total count rate as a function of operating high voltage for the six groups of 7 proportional counters taken with an AmBe(α, n) neutron source in the centre of the cavity of the device in the configuration of Figure 8. All data were taken with the same total measurement time.

Table 6. Total counts for each group of seven proportional counters obtained from measurements with a conventional electronics chain (C_1) and with the A111 board (C_2). The last column is the ratio. All data were taken with the same total measurement time.

Detector group	Conventional electronics C_1	A111 board C_2	C_1/C_2
1	260922	259587	0.995
2	278080	277364	0.997
3	261963	261689	0.999
4	272135	272326	1.001
5	256596	255123	0.994
6	271366	271179	0.999

Figure 17 compares the total count rate as a function of the high voltage resulting from measurements with a ^{252}Cf source and measurements with the same ^{252}Cf source combined with a 8 GBq ^{137}Cs source. The data were taken with the source inside the transfer containers and GT-75 container, as in Figure 12. The data in Figure 17 confirm that for measurements with the A111 board the optimum high voltage in low γ-ray background conditions is around 2100 V. However, they also reveal the reduction of the width of the high voltage plateau due to the increasing γ-ray background.

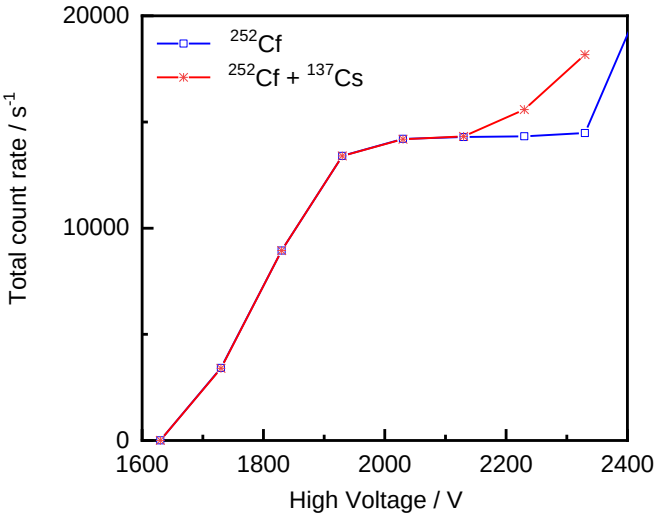

Figure 17. Total count rate as a function of operating high voltage. The results for measurements with a ^{252}Cf(sf) source are compared with those resulting measurements with a ^{252}Cf source and a ^{137}Cs source with a nominal activity of 8 GBq.

7.2 Time dependence

Measurements with a ^{252}Cf(sf) source inside the transfer and GT-75 containers using the CAEN DT5751 digitiser were carried out to determine the time dependence of the response of the neutron detection device. Figure 18 shows a Rossi-alpha distribution from measurements in the configuration of Figure 11 with the ^{252}Cf(sf) source positioned at the bottom of the internal container. The data in Figure 18 show that at least two exponential decay components are needed to describe the time dependence: a main component with a decay constant of 50.6 (2) μs and a second component with decay constant of 119 (4) μs. The relative contributions of these components to the total response are 0.884 (8) and 0.116 (8), respectively. These parameters were derived from a least-squares adjustment to the experimental data. The uncertainties are due to propagating only uncertainties due to counting statistics.

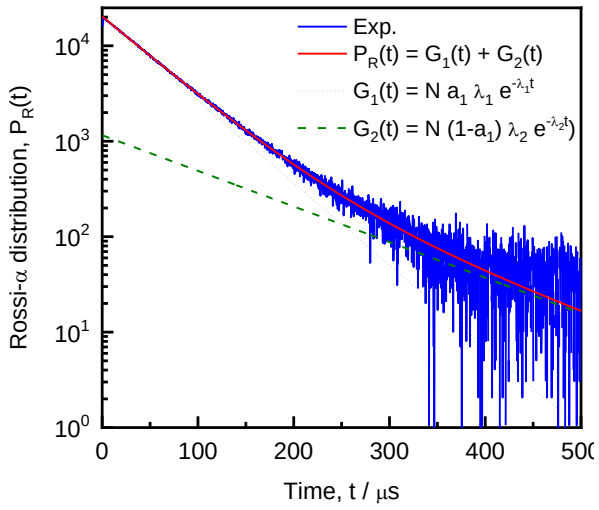

Figure 18. Rossi-alpha distribution from measurements with a ^{252}Cf(sf) neutron source placed in the detection device in the conditions of the configuration in Figure 11. The experimental data are compared with the results of a least-squares adjustment to the data using a sum of two exponential decay components.

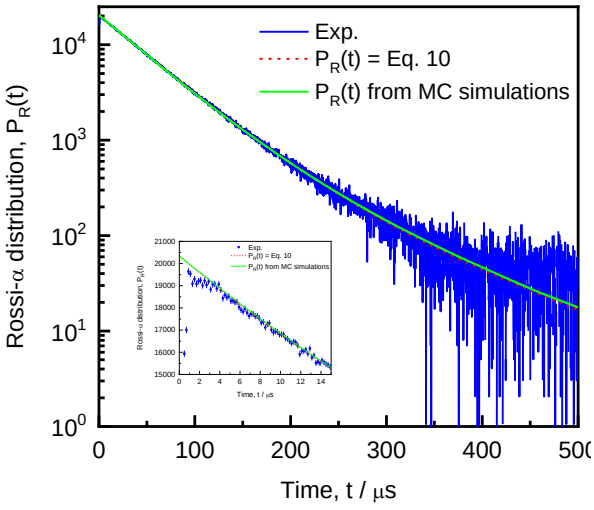

Figure 19. Rossi-alpha distribution from measurements with a ^{252}Cf(sf) neutron source placed in the detection device in the conditions of the configuration in Figure 11. The experimental data are compared with the results of a least squares adjustment to the data using a sum of two exponential decay components and the distribution derived from Monte Carlo simulations combined with the autocorrelation function of Eq. 5.

The deviation from a single exponential decay was confirmed by results of MC simulations. The Rossi-alpha distribution $P_R(t)$ was derived by applying an autocorrelation function:

$$P_R(t)dt = \int g(t')g(t'+t)dt'\ dt\ , \tag{5}$$

with $g(t')dt'$ the probability to detect a neutron at a time between t' and $t'+dt'$ after its creation. The latter was obtained from simulation with MCNP [31]. The energy distribution of prompt fission neutrons from ^{252}Cf(sf) recommended by neutron standards project [36] was used for the calculations. The results of this calculation are shown in Figure 19 and compared with the experimental date after applying a normalisation factor derived from the integrated response between 4.5 µs and 68.5 µs.

7.3 Dead time

To determine the parameters for dead-time corrections, measurements were performed with the output of the detection device connected to a JSR-12 shift register. The shift register was operated with a pre-delay of $t_p = 4.5$ µs and a gate width of $t_g = 64$ µs. Parameters to apply the empirical dead time correction proposed in Ref. [37] were derived from measurements with a set of ^{252}Cf(sf) sources with different intensities. Applying this empirical correction, the measured and dead time corrected totals and reals rates are related by:

$$T_0 \approx T\, e^{(d_1+d_2\,T)T} \tag{6}$$

$$R_0 \approx R\, e^{4\,(d_1+d_2\,T)T} \tag{7}$$

with T and R the measured totals and reals rates, respectively, and T_0 and R_0 the corresponding dead-time corrected rates. The results of these measurements are shown in Figure 20. The experimental data can be reproduced using only the linear term of the exponential exponent, that is, with $d_2 = 0\ (\mu s)^2$. The dead-time parameter $d_1 = 0.250\ (5)$ µs was derived from a least-squares adjustment to the data. The uncertainty results from propagating only uncorrelated uncertainties due to counting statistics.

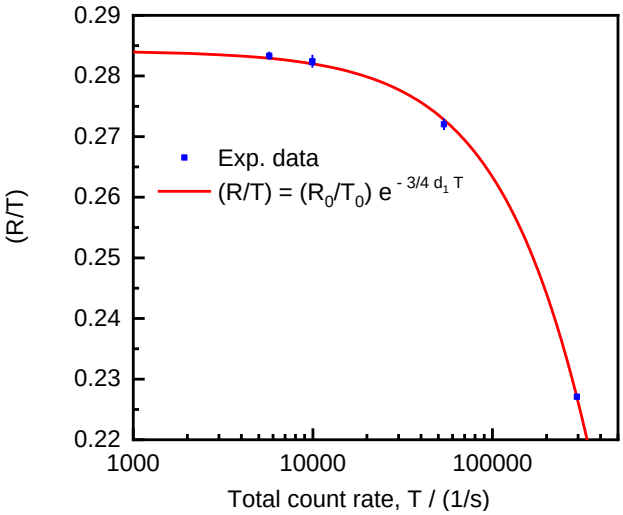

Figure 20. Ratio of the reals and totals rate as a function of the totals rate obtained from measurements in the configuration of Figure 11 using ^{252}Cf sources with different intensities. All sources are sealed in an A3024 capsule type of Eckert & Ziegler [38]. The data are described by combining Eq. 6 and Eq. 7 with $d_1 = 0.250\ (5)$ µs and $d_2 = 0\ (\mu s)^2$.

7.4 Gate fraction and detection efficiency

The detection efficiency of the AWCC counter with the detectors operated at 2100 V and the output connected to the JSR-12 shift register was determined for neutrons originating from an ^{241}AmBe(α, n) source. The source was placed in the centre of the device in the configuration of Figure 8, without the transfer and GT-75 transport containers. Results derived from measurements at JRC-Ispra and JRC-Geel are reported in Table 7. The efficiencies derived from these measurements are within the uncertainty of the declared intensity in very good agreement. The average efficiency $\varepsilon = 0.2116\ (21)$ derived from the experimental data is about 15 % lower compared to the detection efficiency $\varepsilon = 0.249$ derived from Monte Carlo simulations using MCNP. The energy distribution for ^{241}AmBe(α, n) recommended by ISO 8529-1:2001 [39] was used for the simulations.

Table 7. Detection efficiency for neutrons emitted by a ^{241}AmBe(α,n) radionuclide source placed in the centre of the neutron detection device for the configuration shown in Figure 8 with the ^{3}He detectors operating at 2100 V. The detection efficiency is derived from the net total count rate and certified neutron emission rate of the sources. The uncertainties of the experimental efficiencies are dominated by those of the certified intensities.

Source	Laboratory	S_α / s^{-1}	T_0 / s^{-1}	Detection efficiency
4442NK	JRC-Ispra	2.122 (30) × 10^4	4537 (10)	0.2138 (30)
Am 405/13	JRC-Geel	7.711 (110) × 10^4	15102 (30)	0.2090 (30)
				0.2116 (21)

Unfortunately, ^{252}Cf(sf) sources with a certified neutron output were not available at the time of the measurements reported in this work. Therefore, the detection efficiency for prompt fission neutrons from ^{252}Cf(sf) was obtained from a combination of the net totals and reals rate applying the point model presented by Hage and Cifarelli [27]-[30] and Böhnel [40]. Applying this model the detection efficiency ε_{sf} and the production rate for prompt fission neutrons from spontaneous fission S_{sf} can be derived from [41]:

$$T_0 = \varepsilon_{sf}\, S_{sf} \left(1 + r_{\varepsilon,d}\, \frac{\nu_d}{\nu_{sf(1)}}\right) \tag{8}$$

$$R_0 = \varepsilon_{sf}^2\, f\, \frac{\nu_{sf(1)}}{\nu_{sf(2)}}\, S_{sf} \tag{9}$$

with $\nu_{sf(1)}$ the first order and $\nu_{sf(2)}$ the second order normalised factorial moments of the neutron multiplicity distribution. The total number of delayed fission neutrons are denoted by ν_d and the ratio of the detection efficiency for delayed and prompt fission neutrons by $r_{\varepsilon,d}$. The factorial moments and number of delayed neutrons that are recommended for ^{252}Cf(sf) are reported in Table 8. The gate fraction f is the number of detected correlated events within a gate width t_g that is opened at a time t_p after each detected event relative to the number of detected events in the time interval $[0, \infty)$, with $t_p = 0$ and $t_g \to \infty$. Eq. 8 and Eq. 9 are valid for a point source with neutrons produced by spontaneous fission without any neutron multiplication in the source.

Table 8. Half-lives [42], fraction for spontaneous fission [42], normalised factorial moments derived from the multiplicity distribution of the prompt fission neutrons for ^{244}Cm(sf) and ^{252}Cf(sf) in Refs. [43], [44] and delayed neutron emission data from Ref. [45]. The average total number of prompt fission neutrons for ^{252}Cf(sf) resulting from the neutron standards project [36] is also given.

Nuclide	$T_{1/2}$	(sf) fraction	$\nu_{sf(1)}$	$\nu_{sf(2)}$	ν_d	$\nu_d/\nu_{sf(1)}$
^{244}Cm	18.11 (3) a	1.36 (1) 10^{-6}	2.710 (10)	2.971 (37)	0.0033 (10)	1.22 (36) 10^{-3}
^{252}Cf	2.6470 (26) a	3.086 (8) 10^{-2}	3.757 (10)	5.9759 (95)	0.0086 (10)	2.29 (27) 10^{-3}
^{252}Cf			3.7551 (18) [36]			

The gate fraction can be derived from measurements with ^{252}Cf(sf) sources that are certified for their neutron production rate as discussed in Ref. [46]. Unfortunately, at the time the experiments were carried out such sources were not available. Two approaches were applied to estimate the gate fraction. In a first approach the Rossi-alpha distribution was parameterised by a sum of two exponentials:

$$P_R(t) = N\left[a_1\, \lambda_1 e^{-\lambda_1 t} + (1 - a_1)\, \lambda_2 e^{-\lambda_2 t}\right] \tag{10}$$

with the parameters $(N, a_1, \lambda_1, \lambda_2)$ derived from a least-squares adjustment to the experimental data. The gate fraction resulting from such a parameterisation is defined by:

$$f = a_1 e^{-\lambda_1 t_p}\left(1 - e^{-\lambda_1 t_g}\right) + (1 - a_1)\, e^{-\lambda_2 t_p}\left(1 - e^{-\lambda_2 t_g}\right) \tag{11}$$

Note that Eq. 10 is used to parameterise the distribution $P_R(t)$, while in the approaches of e.g. Refs. [47], [48] the probability to detect a neutron at a time t after its creation (i.e. $g(t)$ in Eq. 5) is parameterised by a double exponential decay.

In a second approach the gate fraction was derived directly from the experimentally observed Rossi-alpha distribution as the ratio of integrated counts in the time interval $[t_p, t_p+t_g]$ and the integrated counts in the interval $[0, \infty)$. The contribution of the interval $[0, 4\ \mu s]$ to the counts in the interval $[0, \infty)$ cannot be determined accurately due to dead time effects (see the insert in Figure 19). This contribution, which is about 7 %, was obtained from the parameterised and simulated Rossi-alpha distribution both normalised to the experimental one in the region between 4.5 µs and 68.5 µs. The results of the different approaches are compared in Table 9. Based on these data a gate fraction $f = 0.6195\ (30)$ and $f = 0.6278\ (10)$ was adopted for the configurations without (Figure 8) and with transfer and transport containers (Figure 11), respectively.

Table 9. Results of different approaches to evaluate the gate fraction f for measurements with a ^{252}Cf(sf) point source in the configuration of Figure 8 and Figure 11 and for measurements with the SNF segment sample in the configuration of Figure 11. The uncertainties are only due to propagating uncorrelated uncertainties due to counting statistics.

Analysis approach	Gate fraction, f		
	^{252}Cf Configuration Figure 8	^{252}Cf Configuration Figure 11	SNF segment sample Configuration Figure 11
Analytical (Eq. 11)	0.6240 (15)	0.6268 (5)	0.6317 (5)
Numerical integration exp. data + simulated data for $[0, 4\ \mu s]$	0.6196 (30)	0.6277 (10)	0.6338 (10)
Numerical integration + Eq. 11 for $[0, 4\ \mu s]$	0.6195 (30)	0.6278 (10)	0.6338 (10)
Adopted	0.6195 (30)	0.6278 (10)	0.6338 (10)

The detection efficiency was determined for the configuration without (Figure 8) and with transfer and transport containers (Figure 11). Measurements were carried out at JRC-Ispra using two ^{252}Cf(sf) sources with different intensities. For the analysis a relative detection efficiency $r_{\varepsilon,d} = 1.10$ was assumed. This relative detection efficiency was derived from MC simulations using the energy distribution recommended in Ref. [36] for prompt fission neutrons and the one of ENDF/B-VIII.0 [49] for the delayed neutrons. It should be noted that the impact of the delayed neutrons is extremely small. By neglecting their contribution, the neutron production rate for prompt fission neutrons is overestimated by about 0.2 % and the detection efficiency for prompt fission neutrons underestimated by about 0.1 %.

The results of the analysis are given in Table 10. They are compared with the detection efficiencies derived by MC simulations. The experimental detection efficiency for the conditions of Figure 11 (with the transfer and transport container) is increased by about 4 % compared to the one in the configuration of Figure 8 (without containers). The difference in absolute detection between the experimental and simulated data confirms the overestimation of the detection efficiency derived from MC simulations for neutrons emitted by an AmBe(α, n) neutron source. Previous experiences in modelling such detection devices, see e.g. Ref. [50], shows that relative differences between experimental and calculated detection efficiencies are mostly less than 5 %. Unfortunately, the present detector was constructed in the 90s and documentation to verify the design parameters and technical details about the ^{3}He detectors could not be retrieved. Therefore, it was difficult to identify the origin of the systematic differences [51].

Figure 21 shows the axial dependence of the detection efficiency derived from the totals rate for the measurement conditions of Figure 11. There is an increase in detection efficiency as a function of axial position with a maximum increase of about 3.5 %. There is a good agreement between the axial dependence derived from experimental and simulated data. Due to the axial dependence, the detection efficiency depends on the type of source container and the position of the active material within the container. The detection efficiency for a ^{252}Cf(sf) source in an A3024 capsule type of Eckert and Ziegler [38] changes by 1 % when it is rotated by 180°.

Table 10. Detection efficiency for prompt fission neutrons emitted by a ^{252}Cf(sf) source in the neutron detection device for the configuration without (Figure 8) and with transfer and transport container (Figure 11) and with the detectors operating at 2100 V. The experimental efficiencies are quoted with three uncertainties: only due to propagating uncorrelated uncertainties due to counting statistics (a); propagating in addition the uncertainties of the gate fractions (b) and propagating in addition nuclear data uncertainties (c).

Source	Laboratory	Detection efficiency		Ratio
		Configuration Figure 8	Configuration Figure 11	with/without container Figure 11 / Figure 8
		(a) (b) (c)	(a) (b) (c)	(a) (b)
Q2-991	JRC-Ispra	0.2858 (7) (15) (18)	0.2972 (7) (8) (12)	1.0400 (24) (60)
Q2-987	JRC-Ispra	0.2889 (7) (15) (18)	0.3015 (7) (8) (13)	1.0433 (24) (60)
Average		0.2874 (5) (15) (17)	0.2994 (5) (7) (12)	1.0417 (17) (58)
Standard deviation		0.0022	0.0030	0.0024
MCNP		0.3113 (4)	0.3206 (4)	1.030 (2)
MCNP/Exp.		1.083 (2) (6) (7)	1.071 (2) (3) (5)	0.989 (3) (6)

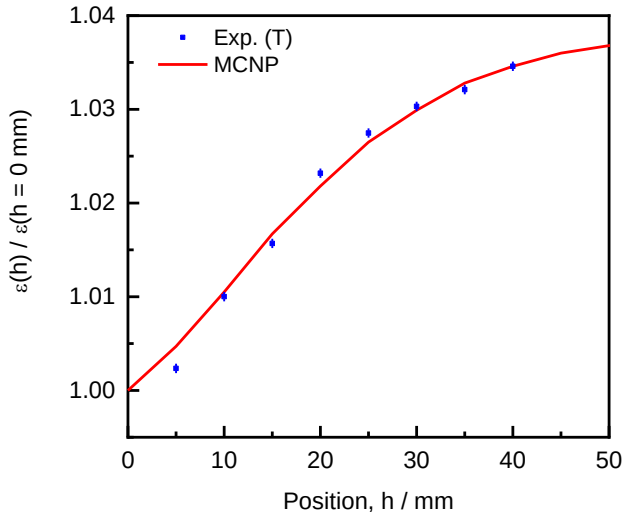

Figure 21. Axial dependence of the detection efficiency for the measurement conditions with transfer and transport container (i.e. configuration of Figure 11). The experimental data obtained with a ^{252}Cf(sf) point source are compared with results obtained by MC simulations. The uncertainties of the experimental data are due to propagating only uncorrelated uncertainties due to counting statistics.

8 Neutron production rate measurements of the SNF segment sample

Finally, measurements of the SNF segment sample described in section 3 were carried out at the LHMA facility of the SCK CEN. First the high voltage plateau with the SNF sample present in the detection device in the conditions of Figure 11 was verified. The results in Figure 22 show a clear reduction in the width of the plateau due to the increased γ-ray background of the SNF sample. To minimise the impact of this background the operating voltage for measurements with the SNF sample was set at the edge of the plateau, i.e. at 2000 V. The resulting efficiency is reduced by about 5 %. This was verified by measurements with ^{252}Cf(sf) sources at JRC-Ispra and SCK CEN based on Eq. 8 and Eq. 9. The results are summarised in Table 11. From these data a weighted average of 0.2852 (10) is derived with a standard deviation of about 0.35 %. This standard deviation is close to the uncertainty due to counting statistics of a single measurement. The uncertainty is the combined standard uncertainty by propagating the uncertainties due to counting statistics, the uncertainty of the gate fraction and the nuclear data uncertainties. This efficiency is for the detection of ^{252}Cf(sf) prompt fission neutrons in the configuration of Figure 11 at the bottom of the inner transfer container with the detectors operated at 2000 V. The production rates of prompt spontaneous fission neutrons at 12h00 UTC on 1st October 2019 derived from the data are reported in Table 12.

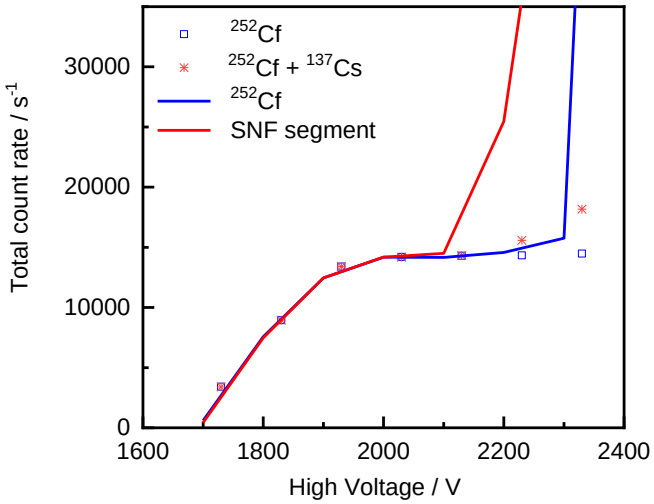

Figure 22. Total count rate as a function of high voltage. Results of the measurement at the LHMA facility (full lines) are compared with those obtained at JRC-Ispra (symbols). The count rates were determined with a ^{252}Cf(sf) source and the SNF segment sample for conditions of the configuration in Figure 11. The data obtained at the LHMA facility are normalised at 2000 V to those obtained at JRC-Ispra.

Table 11. Detection efficiency for prompt fission neutrons emitted by a ^{252}Cf(sf) source in the neutron detection device for the configuration in Figure 11 and with the detectors operating at 2000 V. The sources are contained in an A3024 capsule type container of Eckert and Ziegler [38] and placed at the bottom of the inner container. The efficiencies are quoted with three uncertainties: only due to propagating uncorrelated uncertainties due to counting statistics (a); propagating in addition the uncertainties of the gate fraction (b) and propagating in addition nuclear data uncertainties (c).

Source	Laboratory	Detection efficiency ^{252}Cf(sf) in configuration of Figure 11			
			(a)	(b)	(c)
CN5987	JRC-Ispra	0.2869	(7)	(8)	(12)
CN6001	JRC-Ispra	0.2856	(6)	(8)	(12)
Q2-991	JRC-Ispra	0.2855	(6)	(8)	(12)
Q2-987	JRC-Ispra	0.2843	(6)	(8)	(12)
Q2-988	JRC-Ispra	0.2845	(6)	(8)	(12)
M7-821	SCK CEN	0.2850	(7)	(10)	(14)
Average		0.2852	(3)	(6)	(10)
Standard deviation		0.0010			

Table 12. Prompt fission neutron production rate of ^{252}Cf(sf) sources sealed in an A3025 capsule type of Eckert and Ziegler [38]. The production rates are derived by applying Eq. 8 and Eq. 9. The production rates are quoted with three uncertainties: only due to propagating uncorrelated uncertainties due to counting statistics (a); propagating in addition the uncertainties of the gate fraction (b) and propagating in addition nuclear data uncertainties (c).

Source	Laboratory	Neutron production rate on 1st October 2019				
			(a)	(b)	(c)	
CN5987	JRC-Ispra	2.096	(6)	(7)	(10)	× 10^3
CN6001	JRC-Ispra	1.967	(6)	(7)	(9)	× 10^4
Q2-991	JRC-Ispra	3.420	(10)	(11)	(16)	× 10^4
Q2-987	JRC-ispra	1.870	(5)	(6)	(9)	× 10^5
Q2-988	JRC-Ispra	1.095	(3)	(4)	(5)	× 10^6
M7-821	SCK CEN	1.349	(3)	(4)	(7)	× 10^3

The variation in background and stability of the device with the detectors operated at 2000 V were verified by a set of repeated background measurements and repeated measurements with a ^{252}Cf(sf) neutron source at the LHMA facility of SCK CEN. These measurements were carried out during the night for a total period of 40 days starting at the day that the measurements of the SNF sample was finished and the sample was returned to the hot cell. Results of these repeated measurements are shown in Figure 23. The average background totals and reals rate are 4.25 (16) s^{-1} and 1.07 (8) s^{-1}, respectively. The uncertainties are the standard deviations derived from the repeated measurement data. Results of the 10 repeated measurements with the ^{252}Cf(sf) source are plotted in Figure 24. The standard deviation of the decay corrected intensities is 0.12 %.

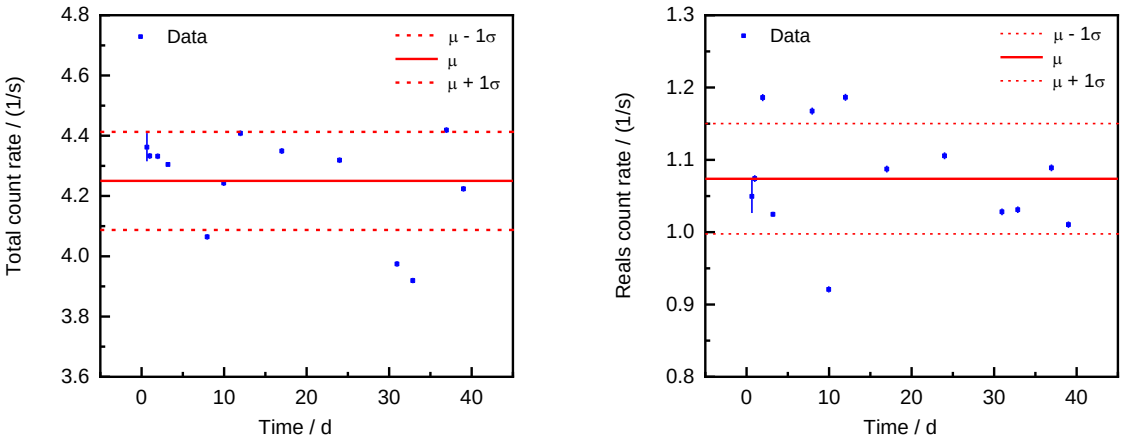

Figure 23. Results of repeated background measurements at the LHMA facility of SCK CEN. The totals (left) and reals rate (right) are shown as a function of the time of measurement. The full line represents the average background rate and the dashed lines are the average plus and minus one standard deviation.

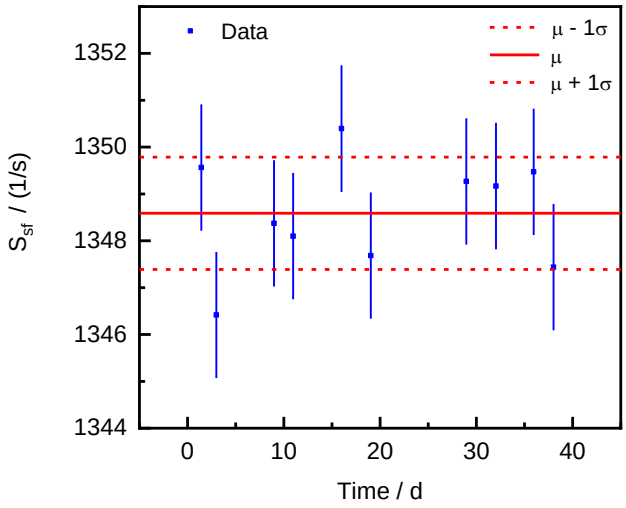

Figure 24. Prompt fission neutron production rate of the M7-821 ^{252}Cf(sf) source of SCK CEN at 12h00 on 1st October 2019 as a function of measurement time. The rates are derived from repeated measurements during a period of 40 days and corrected for the decay using a half-life for ^{252}Cf of $T_{1/2} = 2.645$ years. The full line represents the average production rate and the dashed lines are the average plus and minus one standard deviation. The standard deviation is 0.12 %.

The totals and reals rates resulting from the measurements of the SNF segment sample using the JSR-12 shift register together with the dead time corrections and background contributions are reported in Table 13. The dead time correction for the totals and reals count rate were 1.0019 and 1.0075, respectively, and their background contributions are less than 0.1 %. These data can be used to derive the neutron production rates of the SNF segment sample based on the point-model with the gate fraction as an input parameter; The same procedure as for the measurements with the ^{252}Cf(sf) sources was applied. The Rossi-alpha distribution resulting from measurements with the SNF segment sample using the CAEN DT5751 digitiser is shown in Figure 25. The experimental data are compared with the result of a least squares adjustment using Eq. 10 and the distribution obtained from Monte Carlo simulations. From these data a gate fraction of $f = 0.6338\ (10)$ was derived, with the uncertainty only due to counting statistics.

Table 13. Results of the measurements of the SNF segment sample at the LHMA laboratories of SCK CEN. The observed totals and reals rates and the corresponding count rates corrected for dead time losses and background contributions are given. The uncertainties of the results for the SNF sample are due to propagating the uncertainties due to counting statistics and the background uncertainties. The uncertainties of the background are the standard deviation of repeated measurements.

	Totals			Reals		
	Measured count rate	Dead-time correction	Net count rate	Measured count rate	Dead-time correction	Net count rate
Fuel segment	7465.7 (60)	1.0019	7475.6 (60)	1486.4 (40)	1.0075	1496.6 (40)
Background	4.25 (16)			1.07 (8)		

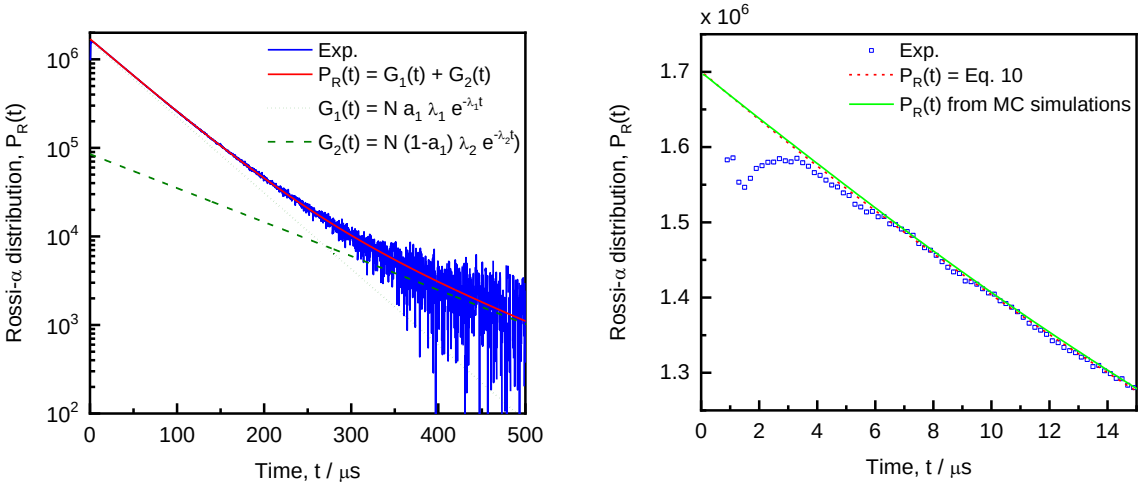

Figure 25. Rossi-alpha distribution for the measurements with the SNF segment sample placed in the detection device in the conditions of the configuration in Figure 11. The experimental data are compared with the results of a least squares adjustment to the data using a sum of two exponential decay components and the distribution derived from MC simulations combined with the autocorrelation function of Eq. 5.

9 Estimation of the neutron production rates of the spent fuel segment

9.1 Model

Following the point model developed in Refs. [27]-[30], [40] and in particular the event tree logic described by Hage and Cifarelli [28], the totals and reals rates resulting from measurements of a SNF sample can be expressed as:

$$T = \varepsilon_{sf}\ S_{sf}\left[\left(l_s + r_{\varepsilon,\alpha}\, l_\alpha\, \alpha + r_{\varepsilon,d}\, l_d\, r_{\nu,d}\right) + r_\varepsilon M\left(p_{Is}\ \nu_{Is(1)} + p_{I\alpha}\ \nu_{I\alpha(1)}\alpha + p_{Id}\ \nu_{Id(1)}\, r_{\nu,d}\right)\right] \quad (12)$$

$$R = \varepsilon_{sf}^2\ f\ S_{sf}\ \frac{\nu_{sf(2)}}{\nu_{sf(1)}}\left[l_s^2 + r_\varepsilon\ 2 l_s\, p_{Is}\ \nu_{Is(1)}\, M + r_\varepsilon^2\left(p_{Is}\ \nu_{Is(1)}\right)^2 M^2\right] + \varepsilon_{sf}^2\, f\, S_{sf}\, r_\varepsilon^2 M^2 \times$$

$$\left[\left(p_{Is}\,\nu_{Is(2)} + p_{I\alpha}\,\nu_{I\alpha(2)}\ \alpha + p_{Id}\,\nu_{Id(2)} r_{\nu,d}\right) + \frac{p\ \nu_{(2)}}{1 - p\ \nu_{(1)}}\left(p_{Is}\,\nu_{Is(1)} + p_{I\alpha}\,\nu_{I\alpha(1)}\ \alpha + p_{Id}\,\nu_{Id(1)} r_{\nu,d}\right)\right] \quad (13)$$

with

- S_{sf} the production rate of prompt fission neutrons from spontaneous fission;
- α the ratio between the production rate of neutrons produced by (α, n) reactions and the production rate of prompt spontaneous fission neutrons;
- $r_{\nu,d}$ the ratio between total number of delayed fission neutrons and prompt spontaneous fission neutrons;
- ε_{sf} the detection efficiency for prompt spontaneous fission neutrons;
- $r_{\varepsilon,\alpha}$ the ratio of the detection efficiency for neutrons produced by (α, n) reactions and prompt spontaneous fission neutrons;
- $r_{\varepsilon,d}$ the ratio of the detection efficiency for delayed fission and prompt spontaneous fission;
- r_ε the ratio of the detection efficiency for prompt fission neutrons from neutron induced and spontaneous fission;
- l_s probability that a prompt spontaneous fission neutron escapes from the sample;
- l_α probability that an (α, n) neutron escapes from the sample;
- l_d probability that a delayed fission neutron escapes from the sample;
- p_{Is} the probability that a prompt spontaneous fission neutron creates an induced fission reaction in the sample;
- $p_{I\alpha}$ the probability that an (α,n) neutron creates an induced fission reaction in the sample;
- p_{Id} the probability that a delayed fission neutron creates an induced fission reaction in the sample;
- p the probability that a prompt fission neutron created by induced fission creates an induced fission reaction in the sample;
- M the leakage multiplication for prompt fission neutrons created by induced fission or the average number of fission neutrons that escape from the sample per first generation prompt fission neutrons;
- $\nu_{sf(1)}$ and $\nu_{sf(2)}$ the first and second order normalised factorial moments of the neutron multiplicity distribution for prompt fission neutrons from spontaneous fission;
- $\nu_{Is(1)}$ and $\nu_{Is(2)}$ the first and second order normalised factorial moments of the neutron multiplicity distribution for prompt fission neutrons due to neutron induced fission by prompt spontaneous fission neutrons;
- $\nu_{I\alpha(1)}$ and $\nu_{I\alpha(2)}$ the first and second order normalised factorial moments of the neutron multiplicity distribution for prompt fission neutrons due to neutron induced fission by (α, n) neutrons;
- $\nu_{Id(1)}$ and $\nu_{Id(2)}$ the first and second order normalised factorial moments of the neutron multiplicity distribution for prompt fission neutrons due to neutron induced fission by delayed fission neutrons;
- $\nu_{(1)}$ and $\nu_{(2)}$ the first and second order normalised factorial moments of the neutron multiplicity distribution for neutron induced fission by prompt fission neutrons from induced fission.

The relation between the leakage multiplication M, the leakage probability l, the probability for neutron induced fission p and the first order factorial moment $\nu_{(1)}$ is given by:

$$M = \frac{l}{1 - p\,\nu_{(1)}}\ . \quad (14)$$

These equations rely on the so-called fast-fission concept [27], which assumes that a fission cascade initiated by primary neutrons, i.e. prompt and delayed neutrons from spontaneous fission and neutrons from (α, n) reactions, is of negligible duration. Hence, it is assumed that neutron multiplication is due to neutron induced fission of fast neutrons and that neutron induced fission by neutrons moderated in the material surrounding the sample can be neglected. In Eq. 12 and Eq. 13 it is supposed that the detection efficiency, escape probabilities and probabilities to create neutron induced fission reactions are the same for all prompt fission

neutrons resulting from neutron induced fission. However, a distinction is made between properties of the primary neutron sources, i.e. prompt and delayed fission neutrons from spontaneous fission and (α, n) neutrons, and those of the prompt neutrons from neutron induced fission cascades. When all neutrons have a similar energy distribution, the detection efficiencies, leakage probabilities, probabilities for fission and neutron multiplicities for prompt neutron induced fission neutrons are in first approximation the same. Under these assumptions and neglecting the contribution of delayed fission neutrons, the expressions in Eq. 12 and Eq. 13 reduce to those of Hage and Cifarelli [28]:

$$T = \varepsilon_{sf}\, S_{sf}\, M\, [\,1 + \alpha\,] \tag{15}$$

$$R = \varepsilon_{sf}^2\, f\, S_{sf}\, M^2 \left[\frac{\nu_{sf(2)}}{\nu_{sf(1)}} + \frac{p\,\nu_{(2)}}{1-p\,\nu_{(1)}}\,(1+\alpha)\right] \tag{16}$$

If in addition, it is assumed that neutrons are only absorbed by neutron induced fission, such that the leakage probability is given by $l = 1 - p$, Eq. 16 becomes [29]:

$$R = \varepsilon_{sf}^2\, f\, S_{sf}\, M^2 \left[\frac{\nu_{sf(2)}}{\nu_{sf(1)}} + \frac{\nu_{(2)}}{\nu_{(1)}-1}\,(M-1)(1+\alpha)\right] \tag{17}$$

Eq. 12 and Eq. 13 were applied to derive the production rate due to spontaneous fission and (α, n) reactions in the SNF segment sample from the totals and reals rates in Table 13. This requires the knowledge of the normalised factorial moments and a prior knowledge of the detection efficiencies, leakage multiplication, escape probabilities and probabilities for neutron induced fission and corresponding normalised factorial moments. The normalised factorial moments for spontaneous fission were obtained from a weighted average of factorial moments recommended in Ref. [44] using a nuclide inventory from depletion calculations with SCALE [52]. The latter are reported in Ref. [53]. The recommended data together with the nuclide inventory and weighted average are given in Table 14. For the sample under investigation the moments are fully determined by those for ^{244}Cm(sf).

Table 14. First and second order normalised factorial moments of nuclides contributing to the production of prompt fission neutrons from spontaneous fission. The data are taken from Ref. [44]. The second order normalised factorial moment for ^{238}Pu is given in Ref. [44] without uncertainties. The average moments are the weighted average based on the relative contributions to the production of prompt fission neutrons in the SNF segment.

Nuclide	Probability for (sf)	$\nu_{sf(1)}$	$\nu_{sf(2)}$
^{244}Cm	0.9739	2.710 (10)	2.971 (37)
^{246}Cm	0.0182	2.930 (30)	3.470 (14)
^{238}Pu	0.0010	2.190 (70)	1.937
^{240}Pu	0.0043	2.154 (5)	1.894 (15)
^{242}Pu	0.0024	2.149 (8)	1.904 (18)
	Average	2.710 (10)	2.972 (37)

The detection efficiency for the SNF segment sample was derived starting from the experimentally determined detection efficiency for a ^{252}Cf(sf) point source at the bottom of the internal container in the configuration of Figure 11 and reported in Table 11. Monte Carlo simulations were performed to account for differences in energy distribution and geometry of the SNF segment sample and to estimate the other parameters, i.e. $M, r_{\varepsilon,\alpha}, r_{\varepsilon,d}, l_{sf}, l_d, p_s, p_\alpha, p_d, p, \nu_{Is(1)}, \nu_{I\alpha(1)}, \nu_{Id(1)}, \nu_{(1)}$. The neutron transport calculations were carried out with MCNP and the nuclide inventory of the SNF sample was obtained from results of depletion calculations reported in Ref. [53]. The first order normalised factorial moments for neutron induced fission $\nu_{I(1)}$ were derived from spectrum averaged values:

$$\nu_{I(1)} = \sum_k w_k \frac{\int N(E)\, \nu_{I(1),k}(E)\, \sigma_{f,k}(E)\, dE}{\int N(E)\, \sigma_{f,k}(E)\, dE} \tag{18}$$

with w_k the relative abundance of nuclide k, $N(E)$ the energy distribution of the incident neutrons creating a neutron induced fission reaction, $\sigma_{f,k}(E)$ the energy dependent fission cross section for nuclide k and $\nu_{I(1),k}(E)$ the corresponding energy dependence of the first order factorial moment (or average number of emitted prompt fission neutrons). For the energy distributions of prompt fission neutrons from neutron induced fission the

energy dependent Watt parameters of Verbeke et al. [54] were used. The second order normalised factorial moments were derived from a parabolic parameterisation of the second order moment as a function of the first order moment, as proposed by Cifarelli and Hage [29]. Such a parameterisation is illustrated in Figure 26. The data were taken from an evaluation of Zucker and Holden [55], which are tabulated in Ref. [54] and rely on the experimental data of Soleilhac et al. [56]. The results of the simulations and calculations to estimate the parameters that are required for the analysis and their impact on the analysis of the data are summarised in Table 15, Table 16 and Table 18 – Table 23.

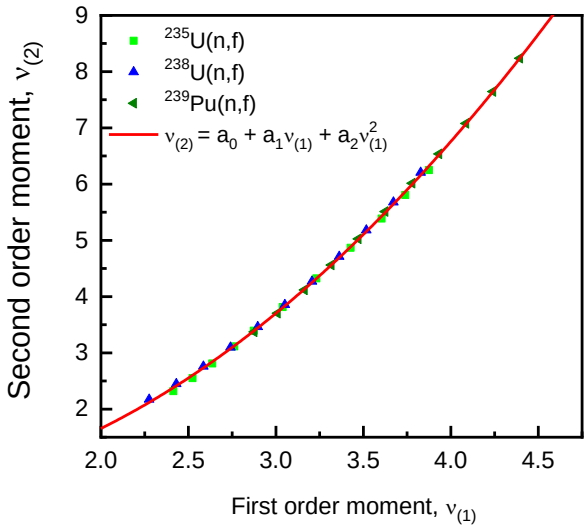

Figure 26. Second order normalised factorial moment as a function of the first order normalised factorial moment derived from the multiplicity distribution for neutron induced fission of ^{235}U, ^{238}U and ^{239}Pu evaluated by Zucker and Holden [55]. The full line is the result of a parabolic parameterisation suggested by Cifarelli and Hage [29]. The parameters ($a_0 = 0.58066$, $a_1 = -0.4701$, $a_2 = 0.5036$) were derived from a fit to the evaluated data.

Table 15 compares the detection efficiency for a ^{252}Cf(sf) cylindrical neutron source with the same dimensions as the SNF segment sample supposing different energy distributions for the emitted prompt spontaneous fission neutrons. The neutron emission probability is homogeneously distributed in the sample. The calculations were carried out without accounting for neutron interactions in the source material. Calculations were performed for the energy distribution of prompt fission neutrons from ^{252}Cf(sf) that is recommended by the standards project [36]. The latter is the result of an evaluation performed by Mannhart [57], [58]. They were repeated using parameterised distributions based on a Watt [59] and a Maxwellian distribution which are given by:

$$N(E) = \frac{e^{-a/b}}{\sqrt{\pi ab}}\, e^{-E/b}\, sinh\left(\frac{2\sqrt{aE}}{b}\right) \tag{19}$$

and

$$N(E) = \frac{2\sqrt{E}}{\sqrt{\pi}(kT)^{3/2}}\, e^{-E/(kT)}, \tag{20}$$

respectively, with E the energy of the prompt fission neutrons, a and b the parameters of the Watt distribution and k and T the Boltzmann constant and temperature, respectively, of the Maxwellian distribution. The parameters a and b of the Watt distribution and the parameter kT of the Maxwellian distribution were adjusted to the recommended spectrum. The results of this adjustment, which are given in Table 15, confirm those obtained by Fröhner [60]. The data in Table 15 show that differences between the detection efficiencies for the recommended and the parameterised spectra are less than 0.1 %. Hence, systematic effects in the simulated detection efficiency due to the assumed energy distribution can be neglected.

Table 15. Simulated detection efficiency for prompt fission neutrons emitted by a ^{252}Cf(sf) source distributed homogeneously in a cylindrical sample with the same dimensions as the SNF segment sample without accounting for neutron interactions in the source material. The third column is the ratio to the efficiency for the energy distribution recommended by the standards project [36]. The uncertainties are only due to the number of simulated neutron histories.

Prompt fission neutron energy distribution: ^{252}Cf(sf) point source	Detection efficiency	Ratio
Recommended, standards project [36]	0.33689 (7)	1
Watt ($\mathrm{a} = 0.462$ MeV, $\mathrm{b} = 1.104$ MeV)	0.33712 (7)	1.0007 (3)
Maxwellian ($kT = 1.45$ MeV)	0.33666 (7)	0.9993 (3)

The detection efficiencies for prompt fission neutrons from ^{252}Cf(sf) in different geometries were simulated to verify the dependence of the detection efficiency on the axial and radial distribution of the neutron emitting material for the configuration of Figure 11. The results are summarised in Table 16. The calculations were performed for a point source at the bottom of the internal transfer container, a line source with the same length as the SNF segment sample and a cylindrical sample with the same dimensions as the SNF segment sample. The calculations for the cylindrical sample were performed for three distributions of the neutron emitting material: neutron emission homogeneously distributed over the volume, neutron emission from the outside surface of the cylinder and a distribution based on a realistic distribution which strongly peaks at the outside of the cylinder. The latter was taken from Ref. [61]. The main difference with the point source geometry is due to dependence of the detection efficiency on the axial distribution of the neutron emitting material. For a sample with the length of the SNF segment sample ($L = 52$ mm) the results of the MC simulations suggest an increase by a factor 1.0236 (15). This increase is fully consistent with an average increase by a factor 1.023 that is derived from the experimental data in Figure 21. The results with the cylindrical sample reveal that differences between detection efficiencies due to different radial distributions of the neutron source are about 0.1 %.

Table 16. Detection efficiency for prompt fission neutrons emitted by a ^{252}Cf(sf) source in different geometrical conditions for the configuration in Figure 11. The third column is the ratio to the efficiency for a point source at the bottom of the internal transfer container. The uncertainties are only due to the number of simulated neutron histories.

Geometrical condition of a ^{252}Cf(sf) neutron source	Detection efficiency	Ratio
Point source at the bottom of the internal transfer container	0.32902 (7)	1
Line source in the centre of the internal transfer container ($L = 52$ mm)	0.33667 (7)	1.0233 (3)
Uniform distributed cylindrical source with the SNF segment dimensions	0.33689 (7)	1.0239 (3)
Source at the outer surface of a cylinder with the SNF segment dimensions	0.33730 (7)	1.0252 (3)
Cylindrical source with the SNF segment dimensions following a distribution that peaks at the outer surface based on Ref. [61]	0.33704 (7)	1.0244 (3)

Similar simulations were carried out starting with prompt fission neutrons from ^{244}Cm(sf), with neutrons produced by (α, n) interactions in the fuel and with delayed fission neutrons. The energy distribution for the prompt fission neutrons was based on the experimental data reported by Boykov et al. [62]. These data were used to determine the parameters of a Maxwellian and Watt distribution. The results of the fit to the data of Boykov et al. [62] are shown in Figure 27. The parameters are given in Table 17. The energy distribution of (α, n) neutrons was parameterised by an analytical function proposed in Ref. [63], which is specified in Table 17. Additional simulations were carried out using the spectrum for (α, n) neutrons derived with the SOURCES 4C code developed at LANL [64], [65]. This code calculates the energy distribution of neutrons produced by (α, n) reactions starting from the α-particle emission spectrum and combining Eq. 3 and Eq. 4. The energy distributions of the (α, n) neutrons based on these approaches are compared in Figure 27 with those of the prompt fission neutrons from ^{244}Cm(sf) and a delayed fission neutron spectrum for ^{252}Cf(sf) taken from ENDF/B-VIII.0 [49].

Table 17. Parameters for a parameterisation of the energy distribution of prompt fission neutrons from ^{244}Cm(sf) by a Maxwellian and Watt distribution. The parameters are derived from a fit to the data of Boykov et al. [62]. The analytical expression describing the energy distribution of neutrons produced by (α, n) in spent UO_2 fuel is taken from Ref. [63].

^{244}Cm(sf)	(α, n) in UO_2 spent fuel	
	Energy region	Distribution
Maxwellian ($kT = 1.39$ MeV)	$E < 0.8$ MeV	$0.2207(E/E_0)^{6.4}$ with $E_0 = 1$ MeV
Watt ($a = 0.620$ MeV, $b = 0.952$ MeV)	0.8 MeV $\leq E < 2.4$ MeV	$-0.3746 + 0.6448E/E_0 - 0.138(E/E_0)^2$
	$E \geq 2.4$ MeV	$0.3803 \exp[-0.77\ (E/E_0 - 2.31)^2]$

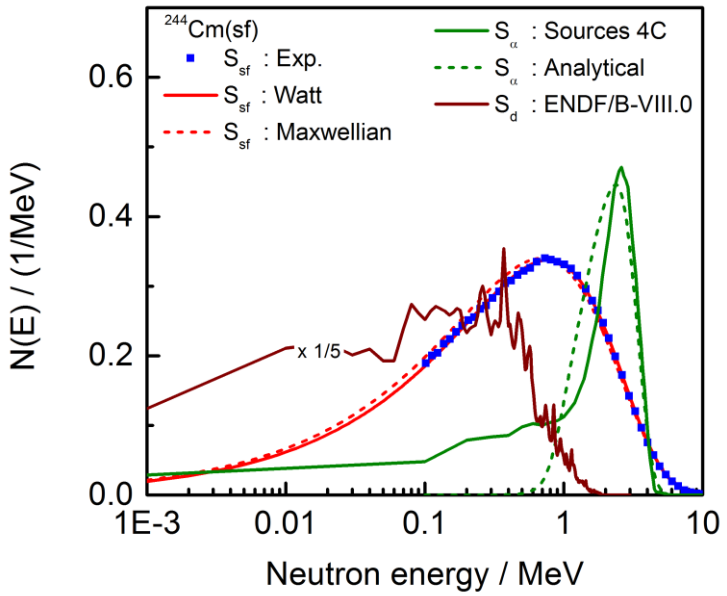

Figure 27. Energy distribution of prompt fission neutrons from ^{244}Cm(sf), (α, n) neutrons and delayed fission neutrons. For ^{244}Cm(sf) the experimental distribution of Boykov et al. [62] is compared with the results of a least squares fit to these data using a Watt and Maxwellian distribution. The analytical expression for the distribution of (α, n) neutrons in Ref. [63] are compared with results of calculations using the SOURCES 4C code [64], [65]. The energy distribution for delayed neutrons for ^{252}Cf(sf)are taken from ENDF/B-VIII.0 [49].

The detection efficiencies for a neutron source homogeneously distributed in a cylindrical sample with the same dimensions as the SNF segment sample using different energy distributions are compared in Table 18. As for ^{252}Cf(sf), the detection efficiency for prompt fission neutrons from ^{244}Cm(sf) does not strongly depend on the parameterisation that is used. The detection efficiency for (α, n) neutrons is reduced by about 3.4 % compared to the one for prompt fission neutrons from ^{244}Cm(sf). The one for delayed neutrons is increased by about 8 %.

Table 18. Detection efficiency for prompt fission neutrons, (α, n) neutrons and delayed fission neutrons distributed homogeneously in a cylindrical sample with the same dimensions as the SNF segment sample without accounting for neutron interactions in the sample material. The third column is the ratio to the calculated efficiency $\varepsilon = 0.32902\ (7)$ for a ^{252}Cf(sf) point source at the bottom of the internal container in the configuration of Figure 11. The uncertainties due to the simulated neutron histories are smaller than the last significant digit.

Energy distribution	Detection efficiency	Ratio with $\varepsilon = 0.32902\ (7)$
^{252}Cf(sf), Watt spectrum (a = 0.462 MeV, b = 1.104 MeV)	0.3371	1.0246
^{244}Cm(sf), Boykov et al. [62]	0.3376	1.0261
^{244}Cm(sf), Watt spectrum (a = 0.620 MeV, b = 0.952 MeV)	0.3378	1.0265
^{244}Cm(sf), Maxwellian spectrum (kT = 1.39 MeV)	0.3379	1.0266
(α,n) distribution (see Table 17)	0.3260	0.9908
(α,n) distribution (SOURCES 4C)	0.3263	0.9918
Delayed fission neutrons (ENDF/B-VIII.0)	0.3645	1.1078

The effect of neutron interactions with the sample material, i.e. spent fuel nuclide inventory and cladding, are summarised in Table 19 – Table 22. Table 19 compares the leakage probability, probability for neutron induced fission and corresponding total average emitted prompt fission neutrons for three energy distributions of primary neutron sources, i.e. neutrons from ^{244}Cm(sf), neutrons from (α, n) reactions and delayed fission neutrons. In addition, the average detection efficiency relative to the one for prompt fission neutrons from ^{244}Cm(sf) is given. The effect of neutrons returning back to the sample after scattering in the material surrounding the sample was verified by performing the calculations with and without the surrounding material. The small difference in fission probability due to the presence of the surrounding material supports the assumption of the fast-fission concept. This is confirmed by the probabilities for neutron induced fission by prompt fission neutrons and (α, n) neutrons as primary neutron sources that are given in Table 20 and Table 21. The results in Table 20 and Table 21 reveal that neutron induced fission is predominantly due to the interaction of fast neutrons with ^{238}U and fast fission is the main neutron absorption process.

Table 19. Leakage and fission probability calculated for three energy distributions of primary neutron sources: prompt fission neutrons from ^{244}Cm(sf), (α, n) neutrons and delayed fission neutrons. The calculations are done considering only the SNF segment sample and with the SNF segment sample in the configuration of Figure 11 to verify the effect of neutron interactions in the sample after neutron scattering in the moderator (or albedo). The uncertainties due to the simulated neutron histories are smaller than the last significant digit.

Energy distribution primary neutron source j	Only SNF sample			SNF sample in detection device			
	l_j	p_{Ij}	$\nu_{Ij(1)}$	l_j	p_{Ij}	$\nu_{Ij(1)}$	$r_{\varepsilon j} = \frac{\varepsilon_j}{\varepsilon_{sf}}$
^{244}Cm(sf) ($j = s$) Watt spectrum	0.9943	0.00428	2.811	0.9939	0.004479	2.806	1
(α,n) ($j = \alpha$) SOURCES 4C	0.9934	0.00605	2.705	0.9929	0.006329	2.703	0.9662
Delayed neutrons ($j = d$) (ENDF/B-VIII.0)	0.9975	0.00041	2.689	0.9970	0.000463	2.690	1.0791

Table 20. Relative probability for neutron induced fission and capture reactions on ^{235,236,238}U and ^{239,240,241}Pu by prompt fission neutrons from ^{244}Cm(sf) in two energy regions: $[0, 0.5\ \mathrm{MeV}]$ and $[0.5\ \mathrm{MeV}, \infty)$. The contributions are given relative to the total absorption probability in the SNF segment sample. The uncertainties due to the simulated neutron histories are smaller than the last significant digit.

Nuclide	Neutron induced fission		Neutron induced capture	
	$\mathrm{E} \leq 0.5\ \mathrm{MeV}$	$\mathrm{E} \geq 0.5\ \mathrm{MeV}$	$\mathrm{E} \leq 0.5\ \mathrm{MeV}$	$\mathrm{E} \geq 0.5\ \mathrm{MeV}$
^{235}U	0.0040	0.0147	0.0009	0.0009
^{236}U	0.0000	0.0083	0.0007	0.0011
^{238}U	0.0001	0.6660	0.0696	0.1247
^{239}Pu	0.0043	0.0209	0.0006	0.0002
^{240}Pu	0.0002	0.0099	0.0005	0.0004
^{241}Pu	0.0009	0.0031	0.0001	0.0002

Table 21. Relative probability for neutron induced fission and capture reactions on ^{235,236,238}U and ^{239,240,241}Pu by (α, n) neutrons in two energy regions: $[0, 0.5\ \mathrm{MeV}]$ and $[0.5\ \mathrm{MeV}, \infty)$. The contributions are given relative to the total absorption probability in the SNF segment sample. The uncertainties due to the simulated neutron histories are smaller than the last significant digit.

Nuclide	Neutron induced fission		Neutron induced capture	
	$\mathrm{E} \leq 0.5\ \mathrm{MeV}$	$\mathrm{E} \geq 0.5\ \mathrm{MeV}$	$\mathrm{E} \leq 0.5\ \mathrm{MeV}$	$\mathrm{E} \geq 0.5\ \mathrm{MeV}$
^{235}U	0.0010	0.0145	0.0002	0.0007
^{236}U	0.0000	0.0093	0.0002	0.0008
^{238}U	0.0000	0.7959	0.0175	0.0962
^{239}Pu	0.0011	0.0207	0.0002	0.0001
^{240}Pu	0.0001	0.0102	0.0002	0.0003
^{241}Pu	0.0002	0.0030	0.0000	0.0001

Characteristics of the prompt fission neutrons that are created in the neutron multiplication process starting with neutron induced fission by prompt fission neutrons from ^{244}Cm(sf), (α, n) neutrons and delayed fission neutrons are given in Table 22. The small difference in fission probability and leakage multiplication between the calculations without and with surrounding material confirms that the equations based on the fast-fission concept can be applied. In addition, differences between the leakage probability, fission probability, leakage multiplication and detection efficiency between neutrons generated by prompt fission neutrons from ^{244}Cm(sf) and (α, n) neutrons are very small. After the second generation no significant change of these quantities is observed. Given the small contribution of delayed neutrons to the multiplication process, the results in Table 22 support the assumptions made in the derivation of Eq. 12 and Eq. 13. The input parameters used for the final analysis are summarised in Table 23.

Table 22. Characteristics for prompt fission neutrons created by neutron induced fission reactions starting with three energy distributions of primary neutron sources: prompt fission neutrons from ^{244}Cm(sf), (α, n) neutrons and delayed fission neutrons. The last column is the detection efficiency relative to the one for prompt fission neutrons from ^{244}Cf(sf). The calculations are done considering only the SNF segment sample and with the SNF segment sample in the configuration of Figure 11. The uncertainties due to the simulated histories are smaller than the last significant digit.

	Only SNF sample				SNF sample in detection device (Figure 11)				
	l	p	$\nu_{(1)}$	M	l	p	$\nu_{(1)}$	M	r_ε
^{244}Cm(sf)									
Generation									
1	0.9946	0.003994	2.789	1.0061	0.9942	0.004190	2.784	1.0062	1.0043
2	0.9946	0.003994	2.789	1.0061	0.9942	0.004190	2.784	1.0062	1.0045
(α, n)									
Generation									
1	0.9946	0.004013	2.791	1.0061	0.9942	0.004209	2.786	1.0062	1.0039
2	0.9946	0.003994	2.789	1.0061	0.9942	0.004190	2.784	1.0062	1.0045
Delayed									
Generation									
1	0.9947	0.003925	2.783	1.0059	0.9943	0.004118	2.778	1.0060	1.0060
2	0.9946	0.003992	2.789	1.0061	0.9942	0.004187	2.784	1.0062	1.0046

Table 23. Input parameter data to derive the neutron production rates from the totals and reals rates using the relations in Eq. 12 and Eq. 13.

Fraction of delayed neutrons			
$r_{\nu,d}$ = 1.22 (36) 10^{-3}			
Normalised factorial moments for spontaneous fission			
$\nu_{sf(1)}$ = 2.710 (10)			
$\nu_{sf(2)}$ = 2.972 (37)			
Detection efficiencies			
ε_{sf} = 0.2926 (10)	$r_{\varepsilon,\alpha}$ = 0.9660	$r_{\varepsilon,d}$ = 1.080	r_{ε} = 1.0045
Gate fraction			
f = 0.6338 (10)			
Leakage multiplication			
M = 1.006			
Leakage probability			
l_s = 0.9943	l_α = 0.9934	l_d = 0.9975	
Probability for neutron induced fission			
p_{Is} = 0.00428	$p_{I\alpha}$ = 0.00605	p_{Id} = 0.00041	p = 0.00400
Normalised factorial moments for neutron induced fission			
$\nu_{Is(1)}$ = 2.811	$\nu_{I\alpha(1)}$ = 2.705	$\nu_{Id(1)}$ = 2.689	$\nu_{(1)}$ = 2.789
$\nu_{Is(2)}$ = 3.239	$\nu_{I\alpha(2)}$ = 2.994	$\nu_{Id(2)}$ = 2.958	$\nu_{(2)}$ = 3.187

9.2 Results

Using the input parameters specified in Table 23 and the experimental data in Table 13 the neutron emission rates due to spontaneous fission and (α, n) reactions were derived. The results are reported in Table 24. The impact of various assumptions that can be made are summarised in Table 25. The data in Table 25 reveal that the production rate due to spontaneous fission is not very sensitive to the assumptions made. This is because the production rate for prompt fission neutrons from spontaneous fission is primarily determined by the reals rate and the contribution of the (α, n) neutrons to the reals rate is very small due to the small multiplication effect. This is illustrated in Figure 28, which plots the production rate of prompt spontaneous fission neutrons that is derived from the totals and reals rate as a function of the α-ratio. On the other hand, the α-ratio can be strongly biased depending on the assumptions made. Neglecting the contribution of delayed neutrons the contribution of (α, n) neutrons will be overestimated by about 4 %, while this contribution will be underestimated by about 7 % when the influence of the difference in energy distribution of the neutrons is not taken into account. The reduction in α-ratio due this assumption is partly compensated by neglecting the contribution of delayed neutrons.

Table 24. Neutron production rate due to spontaneous fission and ratio between neutrons produced by (α, n) reactions and spontaneous fission resulting from an analysis of the totals and reals rates in Table 13 applying Eq. 12 and Eq. 13 using the parameters in Table 23. The uncertainties and correlation coefficient $\rho(S_{sf}, \alpha)$ are the result of a propagation of the uncertainty components specified in Table 26.

S_{sf} / (1/s)	$\alpha = \frac{S_\alpha}{S_{sf}}$	$\rho(S_{sf}, \alpha)$
24505 (375)	0.036 (15)	-0.972

Table 25. Neutron production rate due to spontaneous fission and ratio between neutrons produced by (α, n) reactions and spontaneous fission resulting from an analysis of the totals and reals rates in Table 13. The neutron production rate for spontaneous fission S_{sf} and α-ratio for various assumptions of the input parameters are compared.

Analysis method and assumptions	S_{sf} / (1/s)	$S_{sf}/24505.3$	$\alpha = \frac{S_\alpha}{S_{sf}}$	$\alpha/0.03566$
Eq. 12 and Eq. 13 without assumptions	24505.3	1	0.03566	1
Eq. 12 and Eq. 13 with assumptions				
$r_{\nu,d} = 0$	24504.8	0.99998	0.03703	1.038
$r_{\varepsilon,d} = 1$	24505.3	1.00000	0.03576	1.003
$r_{\varepsilon,\alpha} = 1$	24505.8	1.00002	0.03445	0.966
$r_{\varepsilon} = 1$	24510.9	1.00023	0.03548	0.995
$l_\alpha = l_d = l_s = 0.9943$	24505.3	1.00000	0.03564	0.999
$p = p_\alpha = p_d = p_s = 0.00428$	24509.0	1.00015	0.03567	1.000
$\nu_{(1)} = \nu_{\alpha(1)} = \nu_{d(1)} = \nu_{s(1)} = 2.811$	24504.0	0.99995	0.03569	1.001
Eq. 15 and Eq. 16	24513.5	1.00033	0.03560	0.998
Eq. 15 and Eq. 17	24573.0	1.00276	0.03309	0.928

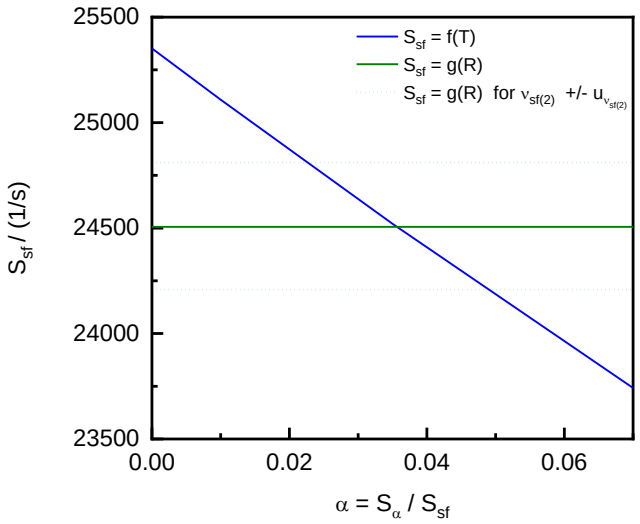

Figure 28. Production rate of prompt fission neutrons due to spontaneous fission S_{sf} as a function of the α-ratio. The production rate derived from the totals and reals rate are plotted separately. The crossing point defines the solution of Eq. 12 and Eq. 13 for S_{sf} and α-ratio. The influence of the uncertainty of the second normalised factorial moment on the production rate and α-ratio is shown by the dotted lines.

The influence of different uncertainty components on the neutron production rate S_{sf} and α-ratio are summarised in Table 26. The sensitivity to the totals and reals rate, the fraction of delayed neutrons, the detection efficiency for prompt spontaneous fission neutrons, gate fraction and first and second order normalised factorial moments of the multiplicity distribution for spontaneous fission was verified together with the sensitivity to input parameters that were derived from Monte Carlo simulations. The sensitivity coefficients are defined by

$$s_{k,j} = \frac{\partial y_k}{\partial x_j} \frac{x_j}{y_k} \qquad (k = 1, 2 \text{ and } j = 1, 2, \ldots 12) \qquad (21)$$

with y_k a quantity of interest and x_j an input parameter, respectively.

For the relative detection efficiencies ($r_{\varepsilon,\alpha}$, $r_{\varepsilon,d}$, r_{ε}) a common relative uncertainty component of 2 % was assumed. The leakage probability was supposed to be the complement of the total probability for fission and capture reactions. To estimate the uncertainties of the fission and capture probabilities they were supposed to be directly proportional to the corresponding cross sections with as main uncertainty component an energy independent normalisation factor of 3 % and 5 %, respectively. For the first and second order factorial moments for neutron induced fission an energy independent relative uncertainty of 1 % and 2 %, respectively, was assumed. The data in Table 26 show that the main uncertainty components are the uncertainties of factorial moments of the multiplicity distribution for prompt spontaneous fission neutrons, the detection efficiency and gate fraction.

Note that the present data are derived starting from the detection efficiency of a ^{252}Cf(sf) point source resulting from measured totals and reals rates in combination with Eq. 12 and Eq. 13. Unfortunately, to our knowledge, no systematic study has been published in the literature evaluating the accuracy of this method based on measurements with ^{252}Cf(sf) sources which are certified for their neutron production rate. For a final analysis additional measurements with ^{252}Cf(sf) sources certified for their neutron production rates are required to produce a reliable estimate of the detection efficiency for prompt fission neutrons from ^{252}Cf(sf) and study possible bias effects of the method applied in this work. Nevertheless, the results presented in this work suggest that the neutron production rate of a SNF sample due to spontaneous fission and related ^{244}Cm inventory can be derived with an uncertainty in the order of 1.5 %, which is close to or even better than the one obtained by radiochemical analysis.

Table 26. Impact of input parameters on the neutron production rate for prompt spontaneous fission neutrons S_{sf} and α-ratio. The sensitivity coefficients ($s_{S_{sf},j}$, $s_{\alpha,j}$) are given together with the relative contributions $\frac{u_{S_{sf},j}}{u_{S_{sf}}}$ and $\frac{u_{\alpha,j}}{u_{\alpha}}$ to the total uncertainty, resulting from the uncertainty u_{x_j} of the input parameter x_j.

Uncertainty component, j	$\frac{u_{x_j}}{x_j}$	$s_{S_{sf},j}$	$s_{\alpha,j}$	$\frac{u_{S_{sf},j}}{u_{S_{sf}}}$	$\frac{u_{\alpha,j}}{u_{\alpha}}$
Totals rate	0.00080	0.02	30.50	< 0.01	0.06
Reals rate	0.0027	1.02	30.50	0.18	0.18
Fraction of delayed neutrons	0.30	0.00	0.04	< 0.01	0.03
Detection efficiency for (sf) neutrons	0.0035	2.02	30.50	0.46	0.23
Gate fraction	0.0016	1.02	30.50	0.11	0.11
First order factorial moment for (sf)	0.0037	1.01	30.08	0.24	0.25
Second order factorial moment for (sf)	0.012	1.01	30.08	0.83	0.83
Relative detection efficiencies	0.02	0.05	0.13	0.07	< 0.01
Neutron induced fission probabilities	0.03	0.03	0.65	0.06	0.04
Neutron induced capture probabilities	0.05	0.00	0.05	0.01	< 0.01
First order factorial moment for (n,f)	0.01	0.02	0.38	0.02	0.01
Second order factorial moment for (n,f)	0.02	0.01	0.42	0.02	0.02

10 Summary and outlook

A procedure to measure the neutron emission rate of a SNF sample by a non-destructive method under standard controlled area conditions was presented. The sample transfer and measurement procedures were described and the results of neutron emission measurements of a SNF segment sample carried out at the LHMA facility of SCK CEN together with a detailed description of the data analysis procedures and uncertainty assessment were discussed.

The measurements were carried out using a neutron well-counter that was designed for routine nuclear safeguards applications. A procedure was defined to transfer a SNF segment sample from the hot cell facilities at the LHMA laboratory of SCK CEN into the detector to minimise the radiation exposure of the operators and avoid a spread of contamination. The procedure was based on the use of a GT-75 transport container of the SCK CEN and additional transfer containers that were adapted to the dimensions of the GT-75 container. The procedure was validated by measurements with a radioactive ^{137}Cs γ-ray source at JRC-Ispra and successfully demonstrated at the SCK CEN using a SNF sample. The sample was a segment taken from a SNF rod that was irradiated in the Tihange 1 PWR reactor to a burnup of 50 GWd/t. The composition and design specifications of this fuel rod and the irradiation conditions are well documented. The SNF segment sample used for the neutron measurements was characterised for its net fuel weight. Additional representative samples were characterised by destructive analysis for different types of investigations such as the inventory of fission products used as BU indicators.

The detection efficiency of the neutron detection device for the measurements of the SNF segment sample was derived by combining measurements with a ^{252}Cf(sf) point source and results of MC simulations. The detection efficiency for the ^{252}Cf(sf) point source was obtained from the totals and reals rate based on the point model proposed by Hage and Cifarelli [27]-[30] and Böhnel [40]. The results of the MC simulations were used to account for the difference in geometry of the SNF segment sample and for the differences in energy distribution with respect to the ^{252}Cf(sf) point source. MC simulations were used to estimate additional effects such as neutron leakage and fission probabilities for different neutron energy distributions. The emission rate of prompt fission neutrons and α-ratio derived from the measured totals and reals rate resulted in $S_{sf} = 24505\ (375)\ \mathrm{s}^{-1}$ and $\alpha = 0.036\ (15)$, respectively. Final estimates of these emission rates require measurements with a ^{252}Cf source certified for its neutron emission rate. These estimates can be used to validate theoretical estimates of the ^{244}Cm abundance in SNF from a combination of neutron transport and fuel depletion calculations.

The performance of the detection device can be improved to reduce the uncertainties and impact of systematic effects. The design of the device and the electronics can be optimised to improve the separation between events due to the detection of neutrons and γ-rays, to reduce the dependence on the axial position, to increase the detection efficiency allowing for an improved multiplicity analysis and to reduce the dead time resulting in a better determination of the gate fraction. Having detailed design specifications and technical details available will improve the results of the MC simulations and reduce bias effects due to correction factors derived from MC simulations.

The results presented in this work are a proof of concept for NDA measurements of SNF samples under standard controlled area conditions. Similar measurements using an optimised device can be carried out to determine the neutron emission rate of samples from other SNF samples including segments from the bottom and top part of the fuel rod and samples from irradiated MOX fuel. Furthermore, the concept to apply NDA on SNF samples outside the hot cell under standard controlled area conditions can be applied for more innovative applications such as Neutron Resonance Transmission Analysis [66] to determine non-destructively the nuclide vector of a SNF sample as an alternative to radiochemical destructive analysis [67].

References

[1] B.L. Broadhead, M.D. DeHart, J.C. Ryman, J.S. Tang and C.V. Parks, “Investigation to Nuclide Importance to Functional Requirements Related to Transport and Long-Term Storage of LWR Spent Fuel”, ORNL Report, ORNL/TM-12742, June 1995

[2] I.C. Gauld, J.C. Ryman and D.D. Ebert, “Nuclide Importance to Criticality Safety, Decay Heating, and Source Terms Related to Transport and Interim Storage of High-Burnup LWR Fuel”, Report NUREG/CR-6700, January 2001

[3] G. Žerovnik, P. Schillebeeckx, K. Govers, A. Borella, D. Ćalić, L. Fiorito, B. Kos, A. Stankovskiy, G. Van den Eynde and M. Verwerft, "Observables of interest for the characterisation of Spent Nuclear Fuel", JRC Technical Reports, EUR 29301 EN, 2018

[4] P. Schillebeeckx, S. Caruso, R. Dagan, L. Fiorito, A. Hernandez Solis, M. Kromar, J. Leppänen, D. Rochman, M. Seidl, A. Stankovskiy, G. Van den Eynde, M. Verwerft and G. Žerovnik, “Characterisation of the nuclide inventory and radiological source terms of spent nuclear fuel: a state-of-the-art report”, JRC Technical Reports, to be published

[5] J. Hu, I.C. Gauld, J.L. Peterson and S.M. Bowman, "US commercial spent nuclear fuel assembly characteristics: 1968 – 2013", Report NUREG/CR-7227, September 2016

[6] I.C. Gauld and C.V. Parks, “Review of Technical Issues Related to Predicting Isotopic Compositions and Source Terms for High-Burnup LWR Fuel”, Report NUREG/CR-6701, January 2001

[7] NEA Nuclear Science Committee, "Spent Nuclear Fuel Assay Data for Isotopic Validation, State-of-the-art Report", Nuclear Science, NEA/NSC/WPNCS/DOC(2011)5, June 2011

[8] H.U. Zwicky, J. Low, M. Granfors, C. Alejano, J.M. Conde, C. Casado, J. Sabater, M. Lloret, M. Quecedo and J.A. Gago, “Nuclide analysis in high burnup fuel samples irradiated in Vandellós 2”, Journal of Nuclear Materials 402 (2010) 60 – 73

[9] I.C. Gauld, J.M. Giaquinto, J.S. Delashmitt, J. Hu, G. Ilas, T.J. Haverlock and C. Romano, “Re-evaluation of spent nuclear fuel assay data for the Three Mile Island unit 1 reactor and application to code validation”, Annals of Nuclear Energy 87 (2016) 267 – 281

[10] J. Hu, J.M. Giaquinto, I.C. Gauld, G. Ilas and T.J. Keever, “Analysis of new measurements of Calvert Cliffs spent fuel samples using SCALE 6.2”, Annals of Nuclear Energy 106 (2017) 221 - 234

[11] D.E. Scatena Wachel, “Radiochemical Analysis Methodology for Uranium Depletion Measurements”, Report DOE/LM-06K140, January 2007

[12] M. Seidl, P. Schillebeeckx and D. Rochman, “On the Potential to Increase the Accuracy of Source Term Calculations for Spent Nuclear Fuel from an Industry Perspective”, accepted for publication in International Journal for Nuclear Power

[13] N. Miura and H.O. Menlove, “The Use of Curium Neutrons to Verify Plutonium in Spent Fuel and Reprocessing Wastes”, LANL Report, LA-12774-MS, May 1994

[14] I.C. Gauld, G. Ilas and G. Radulescu, “Uncertainties in Predicted Isotopic Compositions for High Burnup PWR Spent Nuclear Fuel”, Report NUREG/CR-7012, January 2011

[15] K. Govers “Databook for rods D05 & E12 extracted from assembly FT1X57, Tihange 1 NPP (Rev3), REGAL project”, SCK CEN, report R-6300 (2020)

[16] K. Lemmens, E. González-Robles, B. Kienzler, E. Curti, D. Serrano-Purroy, R. Sureda, A. Martínez-Torrents, O. Roth, E. Slonszki, T. Mennecart, I. Günther-Leopold, Z. Hózer, Instant release of fission products in leaching experiments with high burn-up nuclear fuels in the framework of the Euratom project FIRST- Nuclides, J. Nucl. Mater. 484 (2017) 307-323.

[17] T. Mennecart, G. Leinders, C. Cachoir, G. Cornelis, G. Verpoucke, G. Modolo, D. Bosbach, K. Lemmens, M. Verwerft, First phase of the spent fuel autoclave leaching experiments (SF-ALE) at SCK•CEN, TOPFUEL-GLOBAL 2019, American Nuclear Society, Seattle, (2020) pp. 173-180

[18] M. Verwerft, B. Vos, S. Van den Berghe, K. Govers, First Nuclides Post-Irradiation Examination report Rod D05 - OM1, SCK•CEN, Mol, report R-5579 (2014)

[19] K. Govers, D. Boulanger, K. Meert, G. Leinders and M. Verwerft, “Characterization of Belgian spent fuel assemblies”, SCK•CEN, Mol, Report BLG-1142, (2019)

[20] L. Adriaensen, A. Dobney, Cachoir, “REGAL - Radiochemical Analysis of sample FT1X57-D05-BU1”, SCK CEN, Mol, report R-6375 (2020)

[21] H.O. Menlove, “Description and Operation Manual for the Active Well Coincidence Counter”, LANL Report, LA-7823-M, May 1979

[22] https://www.amptek.com/internal-products/a111-charge-sensitive-preamplifier

[23] B. Pedersen, T. Bogucarska, G. Varasano, L. Holzleitner, K. Ianakiev, M. Iliev, S. Stave, M. Swinhoe, P. De Baere, S. Vaccaro and M. Couland, “Performance evaluation of the KM-200 amplifier in a standard safeguards neutron well-counter”, JRC Technical Reports, EUR 29489 EN, 2018

[24] https://www.caen.it/products/dt5751/
[25] http://www.canberra.com/fr/produits/waste_safeguard_systems/instrumentation.asp
[26] K. Böhnel, “Die Plutoniumbestimmung in Kernbrennstoffen mit der Neutronen-Koinzidenzmethode”, Report KFK-2203, Kerforschungszentrum Karlsruhe, September 1975
[27] W. Hage and D.M. Cifarelli, “Correlation analysis with neutron count distributions in randomly and signal triggered time intervals for assay of special fissile materials”, Nuclear Science and Engineering 89 (1985) 159 – 176
[28] W. Hage and D.M. Cifarelli, “On the factorial moments of the neutron multiplicity distribution of the fission cascades”, Nuclear Instruments and Methods in Physics Research A236 (1985) 165 – 177
[29] D.M. Cifarelli and W. Hage, “Models for a three-parameter analysis of neutron signal correlation measurements for fissile material assay”, Nuclear Instruments and Methods in Physics Research A251 (1986) 550 – 563
[30] W. Hage and D.M. Cifarelli, “Correlation analysis with neutron count distribution for a paralyzing dead-time counter for the assay of spontaneous fissioning material”, Nuclear Science and Engineering 112 (1992) 136 – 158
[31] C. Werner, "MCNP6 User’s Manual, Code version 6.2", Report LA-UR-17-29981, 2017
[32] International Commission on Radiological Protection (ICRP), ICRP Publication 119, Compendium of Dose Coefficients based on ICRP Publication 60, Annals of the ICRP, Vol. 41, Suppl. 1, 2012
[33] J. Leppänen, "Serpent – a Continuous-energy Monte Carlo Reactor Physics Burnup Calculation Code”, User’s Manual, VTT Technical Research Centre of Finland, 2015
[34] J. Leppänen, M. Pusa, T. Viitanen, V. Valtavirta and T. Kaltiaisenaho, ''The Serpent Monte Carlo code: Status, development and applications in 2013”, Annals Nuclear Energy 82 (2015) 142-150
[35] J. Gonzalez, C. Bastian, S. de Jonge and K. Hofmans, “Modular Multi-Parameter Multiplexer MMPM. Hardware description and user guide”, Internal Report GE/R/INF/06/97, IRMM, Geel, 1997
[36] A.D. Carlson, V.G. Pronyaev, R. Capote, G.M. Hale, Z.-P. Chen, I. Duran, F.-J. Hambsch, S. Kunieda, W. Mannhart, B. Marcinkevicius, R.O. Nelson, D. Neudecker, G. Noguere, M. Paris,S.P. Simakov, P. Schillebeeckx, D.L. Smith, X. Tao, A. Trkov, A. Wallner and W. Wang, “Evaluation of the Neutron Data Standards”, Nuclear Data Sheets 148 (2018) 143 – 188
[37] E. Swansen, “Deadtime reduction in thermal neutron coincidence counter”, Nuclear Instruments and Methods in Physics Research B 9 (1985) 80 - 88.
[38] https://www.ezag.com/fileadmin/ezag/user-uploads/pdf/isotope/5_industrial_sources.pdf
[39] ISO 8529-1:2001(en) Reference neutron radiations — Part 1: Characteristics and methods of production
[40] K. Böhnel, “The Effect of Multiplication on the Quantitative Determination of Spontaneously Fissioning Isotopes by Neutron Correlation Analysis”, Nuclear Science and Engineering 90 (1985) 75 – 82
[41] S. Croft and D. Henzlova, “Determining ^{252}Cf source strength by absolute passive neutron correlation counting”, Nuclear Instruments and Methods in Physics Research A 714 (2013) 5 – 12
[42] Data taken from http://www.nucleide.org/DDEP_WG/DDEPdata.htm
[43] N.E. Holden and M. . Zucker, “Prompt neutron multiplicities for the transplutonium nuclides”, Radiation Effects 96 (1996) 289 – 292
[44] P. Santi and M. Miller, “Reevalaution of prompt neutron emission multiplicity distributions for spontaneous fission”, Nuclear Science and Engineering 160 (2008) 190 – 199
[45] A.L. Nichols, D.L. Aldama and M. Verpelli, “Handbook of nuclear data for safeguards: database extensions, August 2008”, IAEA Report, INDC(NDS), August 2008
[46] S. Croft and L.C.-A. Bourva, “The measurement of passive neutron multiplicity counter gate utilization factors and comparisons with theory”, Nuclear Instruments and Methods in Physics Research A 453 (2000) 553 – 568
[47] M.M. Pickrell, N. Ensslin, A. Gavron and H.O. Menlove, “Extensions of neutron multiplicity counting to waste and low-level assay”, Report LA-UR-97-3532, October 1997
[48] L.C.-A. Bourva and S. Croft, “Monte Carlo calculations of the neutron coincidence gate utilization factor for passive neutron coincidence counting”, Nuclear Instruments and Methods in Physics Research A 431 (1999) 485 – 508
[49] D.A. Brown, M.B. Chadwick, R. Capote, A.C. Kahler, A. Trkov, M.W. Herman, A.A. Sonzogni, Y. Danon, A.D. Carlson, M. Dunn, D.L. Smith, G.M. Hale, G. Arbanas, R. Arcilla, C.R. Bates, B. Beck, B. Becker, F. Brown, R.J. Casperson, J. Conlin, D.E. Cullen, M.-A. Descalle, R. Firestone, T. Gaines, K.H. Guber, A.I. Hawari, J. Holmes, T.D. Johnson, T. Kawano, B.C. Kiedrowski, A.J. Koning, S. Kopecky, L. Leal, J.P. Lestone, C. Lubitz, J.I. Márquez Damián, C.M. Mattoon, E.A. McCutchan, S. Mughabghab, P. Navratil, D. Neudecker, G.P.A. Nobre, G. Noguere, M. Paris, M.T. Pigni, A.J. Plompen, B. Pritychenko, V.G. Pronyaev, D. Roubtsov, D. Rochman, P. Romano, P. Schillebeeckx, S. Simakov, M. Sin, I. Sirakov, B. Sleaford, V. Sobes, E.S. Soukhovitskii, I. Stetcu, P. Talou, I. Thompson, S. van der Marck, L. Welser-Sherrill, D. Wiarda, M. White, J.L. Wormald, R.Q. Wright, M. Zerkle,

G. Žerovnik and Y. Zhu, “ENDF/B-VIII.0: The8thMajor Release of the Nuclear Reaction Data Library with CIELO-project Cross Sections, New Standards and Thermal Scattering Data”, Nuclear Data Sheets 148 (2018) 1 – 142

[50] M. Looman, P. Peerani and P. Schillebeeckx, “An overview of NDA Instruments Modelled with the MCNP PTA Code at the JRC Ispra”, Proceedings of the 23rd ESARDA Symposium on Safeguards & Nuclear Material Management, Bruges, Belgium, 8-10 May 2001

[51] P. Schillebeeckx, G. Alaerts, A. Borella, L. Fiorito, K. Govers, J. Paepen, B. Pedersen, A. Stankovskiy, G. Van den Eynde, M. Verwerft, R. Wynants and G. Žerovnik, "Characterisation of spent nuclear fuel by theoretical calculations and non-destructive analysis", Proceedings of the International Workshop on Numerical Modelling of NDA Instrumentation and Methods for Nuclear Safeguards, 16 – 17 May 2018, Luxembourg, pp. 101 – 113

[52] B.T. Rearden and M.A. Jessee, “SCALE Code system, Version 6.2”, ORNL Report, ORNL/TM-2005/39, April 2006

[53] K. Govers, “Databook construction for FIRST-Nuclides & REGAL projects”, Restricted Contract Report SCK•CEN-R-5348, September 2014

[54] J. Verbeke, C. Hagmann and D.M. Wright, “Simulation of Neutron and Gamma Ray Emission from Fission”, Report UCRL-AR-228518, March (2007)

[55] M.S. Zucker and N.E. Holden, “Energy Dependence of the Neutron Multiplicity Pνin Fast Neutron Induced Fission of ^{235,238}U and ^{239}Pu”, BNL Report, Report BNL – 38491, December 1986

[56] M. Soleilhac, J. Frehaut and J. Gauriau, “Energy dependence of $\bar{\nu}_p$ for neutron induced fission of ^{235}U, ^{238}U and ^{239}Pu from 1.3 to 15 MeV”, Journal of Nuclear Energy 23 (1969) 257 – 282

[57] W. Mannhart: in "Properties of Neutron Sources",IAEA-TECDOC-410, IAEA, Vienna (1987) pp. 158 - 170 (1987)

[58] W. Mannhart, “Status of the ^{252}Cf fission-neutron spectrum evaluation with regard to recent experiments”, Proc. Consult. Meeting on Physics of Neutron Emission in Fission (Mito City, Japan, 24–27 May 1988), ed. H.D. Lemmel, pp. 305–336, Report INDC(NDS)-220 (IAEA, Vienna 1989).

[59] D.G. Madland and J.R. Nix, "New calculation of Prompt Fission Neutron Spectra and Average Prompt Neutron Multiplicities" Nuclear Science and Engineering 81 (1982) 213 – 271

[60] F.H. Fröhner, “Evaluation of ^{252}Cf Prompt Fission Neutron Data from 0 to 20 MeV by Watt Spectrum Fit”, Nuclear Science and Engineering, 106 (1990) 345 – 352

[61] C.B. Lee, D.H. Kim, J.S. Song, J.G. Bang and Y.H. Jung, “RAPID model to predict radial burnup distribution in LWR UO_2 fuel”, Journal of Nuclear Materials 282 (2000) 196 – 204

[62] G.S. Boykov, B.G. Gerasimenko, V.D. Dmitriev, L.V. Drapchinsky, O.I. Kostochkin, K.A. Petrzhak, B.M. Shiryaev and V.A. Trenkin, “Precision prompt neutron spectrum measurements of minor actinides for transmutation problem”, Proceedings International Conference on Nuclear Data for Science and Technology, Trieste, Italy, 1997, Vol. 2, pp. 1310, 1997

[63] P.M. Rinard, G.E. Bosler and J.R. Phillips, “Calculated Neutron-Source Spectra from Selected Irradiated PWR Fuel Assemblies”, LANL Report, LA-9125-MS, December 1981

[64] W.B. Wilson, R.T. Perry, E.F. Shores, W.S. Charlton, T.A. Parish, G.P. Estes, T.H. Brown, E.D. Arthur, M. Bozoian, T.R. England, D.G. Madland and J.E. Stewart, “SOURCES 4C: A code for calculating (alpha,n), spontaneous fission and delayed neutron sources and spectra”, LANL Report, LA-UR-02-1839, April 2002

[65] W.B. Wilson, R.T. Perry, W.S. Charlton and T.A. Parish, “Sources: A code for calculating (alpha,n), spontaneous fission, and delayed neutron sources and spectra”, Progress in Nuclear Energy 51 (2009) 608 – 613

[66] P. Schillebeeckx, B. Becker, H. Harada and S. Kopecky, “Neutron resonance spectroscopy for the characterisation of materials and objects”, JRC Science and Policy Reports, Report EUR 26848-EN, 2014

[67] F. Ma, S. Kopecky, G. Alaerts, H. Harada, J. Heyse, F. Kitatani, G. Noguere, C. Paradela, L. Šalamon, P. Schillebeeckx, H. Tsuchiya and R. Wynants, “Non-destructive analysis of samples with a complex geometry by NRTA”, Journal of Analytical and Atomic Spectrometry 35 (2020) 478 – 488

List of abbreviations and definitions

ALARA	As Low As Reasonably Achievable
AWCC	Active Well Coincidence Counter
BU	BurnUp
EURAD	EUropean joint programme on RADioactive waste management
JRC	Joint Research Centre
LANL	Los Alamos National Laboratory
LHMA	Laboratory for High and Medium level Activity
NDA	Non-Destructive Analysis
MC	Monte Carlo
MCNP	Monte Carlo N-Particle
MOX	Mixed OXide
PWR	Pressurized Water Reactor
SCK CEN	Belgian nuclear research centre
SNF	Spent Nuclear Fuel
sf	spontaneous fission
UTC	Coordinated Universal Time

List of figures

List of tables

GETTING IN TOUCH WITH THE EU

In person

All over the European Union there are hundreds of Europe Direct information centres. You can find the address of the centre nearest you at: https://europa.eu/european-union/contact_en

On the phone or by email

Europe Direct is a service that answers your questions about the European Union. You can contact this service:

- by freephone: 00 800 6 7 8 9 10 11 (certain operators may charge for these calls),

- at the following standard number: +32 22999696, or

- by electronic mail via: https://europa.eu/european-union/contact_en

FINDING INFORMATION ABOUT THE EU

Online

Information about the European Union in all the official languages of the EU is available on the Europa website at: https://europa.eu/european-union/index_en

EU publications

You can download or order free and priced EU publications from EU Bookshop at: https://publications.europa.eu/en/publications. Multiple copies of free publications may be obtained by contacting Europe Direct or your local information centre (see https://europa.eu/european-union/contact_en).

KJ-NA-30379-EN-N

The European Commission's science and knowledge service

Joint Research Centre

JRC Mission

As the science and knowledge service of the European Commission, the Joint Research Centre's mission is to support EU policies with independent evidence throughout the whole policy cycle.

EU Science Hub

ec.europa.eu/jrc

@EU_ScienceHub

EU Science Hub - Joint Research Centre

EU Science, Research and Innovation

EU Science Hub

Publications Office of the European Union

doi:10.2760/614853

ISBN 978-92-76-22349-8